gidity, lethargy, cranial nerve palsies, progressive neurological deterioration, hydrocephalus and abscess formation (1). According to the rare descriptions of histopathology associated with CNS MAC, lesions consist of small perivascular aggregates of lymphocytes and macrophages or granulomatous inflammation (1). In the present case, CNS findings on first presentation were non-diagnostic, but suggestive of multiple brain abscesses. Clinical diagnosis of CNS MAC infection is difficult, and most cases of cerebral MAC infection are diagnosed by biopsy or on autopsy (1, 2).

The second CNS presentation of this case occurred in association with pulmonary lesions a few weeks after the start of HAART. This was after the lesions were almost resolved as a result of anti-MAC therapy. While HAART had not brought about significant increases in CD4 T-cell count despite virological response, the clinical course in this case was thought to be complicated by IRIS, because the increase in CD4 T-cell count sometimes might be a delayed response in spite of recovery of other immune function following initiation of HAART and because postmortem pathological findings included granulomatous inflammation which developed at the initial organs of infection with symptoms recurring after initiation of HAART (6-8).

The introduction of HAART for HIV infection has prolonged the lives of patients with AIDS. However, a subgroup of HAART-treated patients is increasingly being recognized that can develop paradoxical clinical, laboratory or radiological deterioration, despite satisfactory control of viral replication and improvements in CD4 T- lymphocyte counts. This phenomenon has been called IRIS. Consistent diagnostic criteria and standards of therapy are yet to be defined, but this condition results from an exuberant inflammatory response towards previously diagnosed or incubating opportunistic pathogens, as well as responses towards other as-yet-undefined antigens due to restored immune function by HAART (6-8).

MAC is frequently reported as a causative pathogen in IRIS. MAC-related IRIS most commonly presents with localized lymphadenitis/lymphadenopathy or pulmonary disease. Localized involvements of the musculoskeletal system, intra-abdominal organs and CNS are less frequently described. Histopathological examination of the lesions often reveals granulomatous inflammation. MAC is usually cultured from granulomatous and/or necrotizing lesions, and the organisms are surrounded by intense inflammatory response in these lesions on pathological examination (2, 7, 9). However, the presumed organisms could not be identified by culture or other diagnostic methods in some cases due to the pathogen-specific intense inflammation rather than actual reactivation of the infection. Most cases display generally favorable outcomes without any additional treatment other than anti-mycobacterial drugs, and when inflammation threatens significant morbidity or mortality, anti-inflammatory measures are considered (7, 9).

The present case was peculiar in that findings of MAC were not demonstrated by morphological, microbiological or nested PCR DNA amplification approaches from lesions, and clinicopathological features showed granulomatous ventriculo-encepalitis with necrosis. The pathogenesis of this case was likely the result of an exuberant inflammatory response toward dead or dying organisms or residual antigen in the original infected organs.

MAC-related IRIS may be clinically indistinguishable from active infection, and might be benign and self-limiting, or severe as in this case. While immune reconstitution remains a therapeutic goal in patients with HIV infection, the very same phenomenon can ironically result in a heightened immune response, causing tissue destruction and subsequent exacerbation of the disease. This may be more apparent in the brain, where the phenomenon can be fatal. The significance of positive EBV PCR in CSF obtained at autopsy in the present patient was probably an incidental pathological finding related to primary CNS lymphoma. IRIS plays a role in several AIDS-related CNS disorders, such as tuberculosis, cryptococcal disease, HIV encephalitis and progressive multifocal leucoencephalopathy (10). Proper recognition of this syndrome is essential, as antiretroviral therapy is increasingly being used worldwide, and IRIS may thus emerge as an important neurological complication of HIV and HAART.

References

1. Gyure KA, Prayson RA, Estes ML, Hall GS. Symptomatic mycobacterium avium complex infection of the central nervous system. A case report and review of the literature. Arch Pathol Lab Med **119**: 836-839, 1995.
2. Murray R, Mallal S, Heath C, French M. Cerebral mycobacterium avium infection in an HIV-infected patient following immune reconstitution and cessation of therapy for disseminated mycobacterium avium complex infection. Eur J Clin Microbiol Infect Dis **20**: 199-201, 2001.
3. Inderlied CB, Kemper CA, Bermudez LE. The Mycobacterium avium complex. Clin Microbiol Rev **6**: 266-310, 1993.
4. Hocqueloux L, Lesprit P, Herrmann JL, et al. Pulmonary Mycobacterium avium complex disease without dissemination in HIV-infected patients. Chest **113**: 542-548, 1998.
5. Levy RM, Bredesen DE. Central nervous system dysfunction in acquired immunodeficiency syndrome. J Acquir Immune Defic Syndr **1**: 41-64, 1988.
6. Shelburne SA, Hamill RJ, Rodriguez-Barradas MC, et al. Immune reconstitution inflammatory syndrome: emergence of a unique syndrome during highly active antiretroviral therapy. Medicine (Baltimore) **81**: 213-227, 2002.
7. Lawn SD, Bekker LG, Miller RF. Immune reconstitution disease associated with mycobacterial infections in HIV-infected individuals receiving antiretrovirals. Lancet Infect Dis **5**: 361-373, 2005.
8. Robertson J, Meier M, Wall J, Ying J, Fichtenbaum CJ. Immune reconstitution syndrome in HIV: Validating a case definition and identifying clinical predictors in persons initiating antiretroviral therapy. Cli Infect Dis **42**: 1639-1648, 2006.
9. Phillips P, Bonner S, Gataric N, et al. Nontuberculous mycobacterial immune reconstitution syndrome in HIV-infected patients:

spectrum of disease and long-term follow-up. Clin Infect Dis **41**: 1483-1497, 2005.

10. Riedel DJ, Pardo CA, McArthur J, Nath A. Therapy insight: CNS manifestations of HIV-associated immune reconstitution inflammatory syndrome. Nat Clin Pract Neurol **2**: 557-565, 2006.

Cellular/Molecular

Regulation of Axonal Elongation and Pathfinding from the Entorhinal Cortex to the Dentate Gyrus in the Hippocampus by the Chemokine Stromal Cell-Derived Factor 1α

Yoichi Ohshima,[1,2,3] Takekazu Kubo,[2] Ryuta Koyama,[4] Masaki Ueno,[1,2] Masanori Nakagawa,[3] and Toshihide Yamashita[1,2]

[1]Department of Molecular Neuroscience, Graduate School of Medicine, Osaka University, Osaka 565-0871, Japan, [2]Department of Neurobiology, Graduate School of Medicine, Chiba University, Chiba 260-8670, Japan, [3]Molecular Neurology and Gerontology, Kyoto Prefectural University of Medicine, Kyoto 602-8566, Japan, and [4]Laboratory of Chemical Pharmacology, Graduate School of Pharmaceutical Sciences, The University of Tokyo, Tokyo 113-0033, Japan

During the early developmental stage, a neural circuit is established between the entorhinal cortex (EC) and the hippocampal dentate gyrus (DG) via the perforant pathway. However, the manner in which the perforant fibers are navigated has mostly remained a mystery. Here, we analyzed the functional role of a chemokine, namely, stromal cell-derived factor 1α (SDF-1α), in the navigation of the perforant fibers. SDF-1α was observed to promote neurite growth, which is dependent on mDia1, in cultured entorhinal cortical neurons obtained from rats at postnatal day 0. We then used entorhino-hippocampal cocultures comprising green fluorescence-labeled EC and DG slices to assess the projection of the perforant fibers from the EC. Although the specific laminar termination of the entorhinal axons was observed with this system, the number of appropriately terminating entorhinal axons decreased significantly when the SDF-1α signaling pathway was blocked by a neutralizing antibody against SDF-1α or by the specific SDF-1α receptor antagonist AMD3100 (1,1′-[1,4-phenylenebis(methylene)]bis-1,4,8,11-tetra-azacyclotetradecane octahydrochloride). Furthermore, inhibition of the SDF-1α signaling pathway resulted in a decrease in the immunoreactivity for PSD-95 (postsynaptic density protein-95) in the DG, possibly because of a reduction in the number of projecting perforant fibers. These results demonstrate that SDF-1α plays a critical role in promoting the growth of perforant fibers from the EC to the DG.

Key words: **stromal cell-derived factor-1; CXCR4; hippocampus; dentate gyrus; entorhinal cortex; axonal elongation; slice culture; cell culture**

Introduction

The entorhino-hippocampal circuitry comprises neurons originating in the entorhinal cortex (EC) and functions as the major excitatory input to both the ipsilateral and contralateral hippocampus/dentate gyrus (DG). This fiber tract comprises projections of the alveolar and perforant pathways and a commissural projection (Skutella and Nitsch, 2001). The perforant fiber extends from the EC to the DG. The afferent pathway arising from EC layer II is one of the major inputs in the DG. Recent studies have provided evidence of the involvement of various membrane-associated attractive or repulsive axon guidance molecules in hippocampal development. For example, the secreted semaphorins and their binding partners, neuropilins, regulate the development of hippocampal fiber projections (Chen et al., 2000; Gu et al., 2003). Plexins are receptors implicated in mediating semaphorin signaling and regulating the development of hippocampal axonal projections (Cheng et al., 2001). Other molecules, including ephrins (Stein et al., 1999), netrins (Steup et al., 2000), Slits (Nguyen Ba-Charvet et al., 1999), and ECM (extracellular matrix) molecules (Zhao et al., 2003), have been reported to regulate the development of hippocampal circuitry. Although it has been demonstrated that the repulsive guidance molecule a (RGMa) repels the perforant fibers causing them to terminate at the outer molecular layer of the DG (Brinks et al., 2004), the factors inducing the elongation of the perforant fibers from the EC to the DG remain to be elucidated.

Stromal cell-derived factor 1α (SDF-1α) is a chemokine that plays an important role in blood formation (Ara et al., 2005). CXCR4, an SDF-1 receptor, mediates the migration of leukocytes and hematopoietic progenitors (Zou et al., 1998). CXCR4 is known to function as a receptor for HIV-1 (type 1 human immunodeficiency virus) in host cells and is an indispensable molecule for the appearance of AIDS (acquired immunodeficiency syndrome) (Bleul et al., 1997). In the neuronal system, SDF-1α and CXCR4 regulate neural migration and axonal pathfinding (Lieberam et al., 2005; Stumm and Höllt, 2007) and play a critical role in the migration of cerebellar granule neurons during the early developmental stages (Ma et al., 1998; Vilz et al., 2005).

Received Dec. 23, 2007; revised June 24, 2008; accepted June 30, 2008.

This work was supported by National Institute of Biomedical Innovation Research Grant 05-12 and a Grant-in-Aid for Young Scientists (S) from Japan Society for the Promotion of Science (T.Y.).

Correspondence should be addressed to either of the following: Toshihide Yamashita or Takekazu Kubo, Department of Molecular Neuroscience, Graduate School of Medicine, Osaka University, 2-2 Yamadaoka, Suita, Osaka 565-0871, Japan. E-mail: yamashita@molneu.med.osaka-u.ac.jp or kubo@restaff.chiba-u.jp.

DOI:10.1523/JNEUROSCI.1670-08.2008

 0270-6474/08/288344-10$15.00/0

SDF-1–CXCR4 signaling regulates the migration of sensory neuron progenitors to the dorsal root ganglion (Belmadani et al., 2005). Furthermore, it has been demonstrated that the migration of hippocampal dentate granule cells from the ventricular zone to the hippocampus is inhibited in *CXCR4*-knock-out mice (Bagri et al., 2002; Lu et al., 2002). SDF-1α signaling is also required for normal cortical development (Paredes et al., 2006; Li et al., 2008). Moreover, SDF-1α has been shown to enhance the axonal branching of hippocampal neurons derived from rats at postnatal day 18 (Pujol et al., 2005). These data demonstrate that the signaling pathway involving SDF-1α and CXCR4 plays an essential role in neuronal development. In the present study, we assessed the possible involvement of SDF-1α and its receptor in the navigation of perforant fibers from the EC to the DG. To test this hypothesis, we used rat entorhino-hippocampal slice cultures because mice with *SDF-1* or *CXCR4* gene deletions were not an ideal model for our experiments. *CXCR4*-knock-out mice exhibit a defect in the structure of the dentate granule cell layer because of poor migration of the granule cells (Bagri et al., 2002; Lu et al., 2002). By performing a series of experiments, we observed that SDF-1α was involved in the elongation of the perforant fiber from the EC to the DG in the slice culture system.

Materials and Methods

Reagents. The rabbit anti-SDF-1 (1:200) and anti-CXCR4 (SDF-1 receptor; 1:200 for the immunohistochemistry and 1:1000 for Western blot analysis) antibodies were obtained from Torrey Pines Biolabs. The rabbit anti-Rho-associated kinase α (ROKα) antibody (1:500) was obtained from Millipore. The mouse anti-neuronal nuclear (NeuN) monoclonal antibody (1:500) was obtained from Millipore Bioscience Research Reagents. Goat anti-mouse or -rabbit IgG (H+L) conjugated to Alexa Fluor 488 (1:400 for the slice culture and 1:1000 for the dissociated culture) or Alexa Fluor 568 (1:400 for the slice culture and 1:1000 for the dissociated culture) or Alexa Fluor 405 (1:400 for the slice culture) was procured from Invitrogen. Recombinant mouse CXCL12/SDF-1α and the anti-human/mouse CXCL12/SDF-1 antibody were obtained from R&D Systems. 1,1′-[1,4-Phenylenebis(methylene)]bis-1,4,8,11-tetra-azacyclotetradecane octahydrochloride (AMD3100 octahydrochloride hydrate), a specific SDF-1-receptor antagonist, was obtained from Sigma-Aldrich. Polyclonal anti-RGMa antibodies (1:100) were produced in our laboratory (Hata et al., 2006) and obtained from Immunobiological Laboratories. The rat mDia1 short interfering RNA (siRNA) (GeneID 307483) and the control siRNA 1 were obtained from Dharmacon Research. The control siRNA 2 was obtained from Sigma-Aldrich (SiPerfect Negative Control). The mouse mDia1 antibody (1:500) was obtained from BD Biosciences. (*R*)-(+)-*trans*-*N*-(4-pyridyl)-4-(1-aminoethyl)-cyclohexanecarboxamide, 2HCl (Y-27632) was obtained from Calbiochem. The neuronal class III β-tubulin (Tuj1) mouse monoclonal antibody (1:1000) was obtained from Covance. The rabbit anti-Prox1 polyclonal antibody (1:1000), used for labeling dentate granule neurons, and the mouse anti-postsynaptic density protein 95 (PSD-95) monoclonal antibody (1:500), used for labeling the postsynaptic membrane, were procured from Millipore Bioscience Research Reagents. The rabbit polyclonal anti-green fluorescent protein (GFP) antibody (1:500) was obtained from Abcam. 1,1′-Dioctadecyl-3,3,3′,3′-tetramethylindocarbocyanine perchlorate (DiI) was obtained from Invitrogen.

Immunohistochemistry. Brain cryosections (thickness, 10 μm) of rats at postnatal day 0 were prepared. The primary antibodies used were rabbit anti-SDF-1 (1:200), rabbit anti-CXCR4 (1:200), and mouse anti-NeuN (1:500) antibodies. The secondary antibodies used were goat anti-mouse or -rabbit IgG conjugated with Alexa Fluor 488 (1:1000) or Alexa Fluor 568 (1:1000). The sections were treated with 5% bovine serum albumin (BSA) and 0.1% Triton X-100 in PBS for 30 min. After the sections were washed three times in PBS, they were allowed to react with the primary antibodies overnight at 4°C. The sections were washed three times and allowed to react with the secondary antibodies for 1 h at room temperature. They were then observed under a fluorescence microscope (Eclipse E600; Nikon).

In situ *hybridization.* The SDF-1α antisense and the sense riboprobes were generated by transcription of a mouse CXCR4 reading frame region cloned into a pCMV-SPORT 6 (Invitrogen; MGC clone 2864967). The brains of the rats at postnatal day 0 were perfused with 4% paraformaldehyde (PFA) for 2–3 d at 4°C, and then perfused with 30% sucrose/PFA until they sank. The brains were then frozen at −80°C and sectioned at 60 μm on a cryostat. The sections were processed for nonradioactive *in situ* hybridization as described previously (Shimogori et al., 2004).

Cell culture of entorhinal neurons. Entorhinal cortical neurons were obtained from rats at postnatal days 0–1 and were processed as described previously (Hata et al., 2006). The dissociated neurons were plated at 8.0×10^4 cells/cm^2 in slide chambers coated with poly-L-lysine in serum-free DMEM supplemented with B27 (Invitrogen). The neurons were incubated for 1 d in the absence or presence of 400 ng/ml SDF-1α. Where indicated, they were coincubated with 15 μg/ml AMD3100, 60 μg/ml anti-SDF-1 antibody, the anti-RGM antibody (1:100), or 1 μg/ml RGMa. The neurons were also incubated in various concentrations of SDF-1α (10, 25, 100, 400, and 1000 ng/ml) and RGMa (0.2, 1.0, 2.0, and 4.0 μg/ml). The neurons were fixed in 4% PFA for 20 min and blocked for 30 min in PBS containing 5% BSA and 0.1% Triton X-100. Tuj1 was used to label the neurites, and the immunoreactivity was detected by using Alexa Fluor 488-conjugated anti-mouse IgG. The neurons were randomly photographed. Their axon lengths and the number of neurites and branches per neuron were measured. Approximately 50 cells per well and three to four wells per experiment were analyzed.

Knockdown of mDia1. The short interfering double-stranded RNA oligomers (siRNA) for mDia1 (20 μM) or the control siRNAs (20 μM) in nucleofactor solutions (100 μl) was transfected into the entorhinal cortical neurons (1 ml; 4×10^6 cells/ml) using the NucleofectorII Device (Amaxa Biosystems). Then, the cells were plated on 35 mm dishes (for Western blot, at 4.0×10^4/cm^2) or slide chambers (for the neurite growth assay, at 8.0×10^4/cm^2) coated with poly-L-lysine, and incubated in the DMEM including 10% FBS (2×10^5/ml) for 1 or 2 d. Where indicated, the neurons were incubated for a day in the absence or presence of 400 ng/ml SDF-1α and/or 50 μM Y-27632.

Western blot analysis. The neurons were lysed in a lysis buffer containing 50 mM HEPES, 1% NP-40, 5% glycerol, 150 mM NaCl, 10 μg/ml leupeptin, and 10 μg/ml aprotinin. The samples were centrifuged at 15,000 rpm for 5 min, and the supernatant was collected. One-half of the volume of 2× SDS buffer was added to the samples. The mixtures were boiled for 3 min and subjected to SDS-PAGE and Western blot analysis using the anti-mDia1 antibody (1:500), the anti-ROKα antibody (1:500), and the anti-CXCR4 antibody (1:1000).

Slice culture. Neurons obtained from the EC of a GFP transgenic rat (Okabe et al., 1997) or a normal rat and from the hippocampus of a normal rat were used for coculturing (Koyama et al., 2004a). All the brain specimens used were obtained from rats at postnatal days 0–1. The brains were sliced into 300-μm-thick sections on a vibratome (DTK-1000 zero1; Dosaka). The slices were cultured on sterilized culture plate inserts (Millicell) in a minimal essential medium supplemented with 20 mM HEPES buffer and 20% horse serum (Koyama et al., 2004a,b). An entorhinal cortical slice and a hippocampal slice were exactly placed to monitor the projection of the perforant fibers from the EC to the DG (see Figs. 1, 5*A*). The slices were incubated for 9 d in the absence or presence of 50 μg/ml AMD3100, 60 μg/ml anti-SDF-1 antibody, or 10 μg/ml anti-RGM antibody. Furthermore, the slices were fixed in 4% PFA overnight and permeabilized in 0.1 M phosphate buffer (PB) containing 0.4% Triton X-100 overnight. The tissues were blocked for 1 h with 0.1 M PB containing 2% goat serum at room temperature and stained with primary antibodies diluted in 0.1 M PB containing 2% goat serum at 4°C overnight. The primary antibodies used were the mouse anti-NeuN (1:200), rabbit anti-Prox1 (1:1000), anti-GFP (1:500), anti-CXCR4 (1:200), and anti-PSD-95 (1:500) antibodies. The tissues were incubated at 4°C overnight with the secondary antibodies conjugated with Alexa Fluor 568 (1:400), Alexa Fluor 488 (1:400), or Alexa Fluor 680 (1:400). They were then mounted on glass slides and observed under a confocal fluorescence microscope (IX81; Olympus). The GFP fluorescence intensities of the

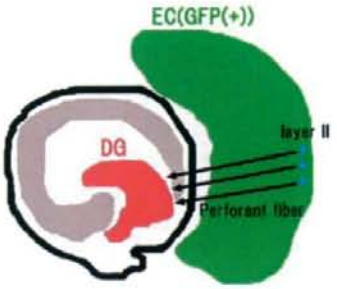

Figure 1. The perforant fibers project from the entorhinal cortex to the dentate gyrus. The perforant fibers emerge from the EC and project to the DG. To analyze the projection of these fibers from the EC to DG, we used rat slice culture systems comprising the EC of a GFP transgenic rat and the hippocampus of rats at postnatal days 0–1. The tissues were sliced to a thickness of 300 μm, and the slices were cocultured for 9 d. The neurons (layer II) in the EC (green) project axons to the DG (arrows).

perforant fibers were measured in eight fields of 25 μm^2 each; the ratios of the intensities of the perforant fibers to the intensities in the EC were calculated, and each value was averaged. Moreover, the fluorescent points labeled with the anti-PSD-95 antibody and/or anti-GFP antibody was counted in five different fields with an area of 100 μm^2 for each sample.

DiI back-labeling of the perforant fibers. The slice tissues were immunostained with the anti-CXCR4 antibody and incubated at 4°C overnight with the secondary antibodies conjugated with Alexa Fluor 405 (1:400). Separately, a glass pin coated with the lipophilic carbocyanine dye, DiI, was placed in the DG in the samples of the slice to label the perforant fibers (see Fig. 8*A*). The samples were incubated for 3–4 d to allow diffusion in 4% PFA at 37°C.

Statistical analysis. One-way ANOVA followed by Scheffe's multiple-comparison test was applied to compare the average values for axon length, fluorescence intensity, or the number of fluorescent points. Values of $p < 0.05$ were considered significant. The statistics repeated from experiment to experiment are used in the experiments using the dissociated cell cultures (see Figs. 3, 4), and the statistics based on the entire cumulative data set are used in the experiments using the slice cultures (see Figs. 5, 7).

Results

SDF-1α is distributed in the DG of the hippocampus, and its receptor, CXCR4, is expressed in the EC

To analyze the navigation of perforant fibers from the EC to the DG, we used rat slice culture systems (Figs. 1, 5*A*). Because *CXCR4*-knock-out mice exhibit a defect in the structure of the dentate granule cell layer as a result of poor migration of the granule cells (Bagri et al., 2002; Lu et al., 2002), we used a previously established explant culture system (Koyama et al., 2004a,b). This system comprises slices of the EC of GFP transgenic rats and the hippocampus of normal rats obtained on postnatal days 0–1. These 300-μm-thick slices were cocultured for 9 d. The navigation of entorhinal axons can be clearly visualized with this culture system.

First, we attempted to assess the possible involvement of SDF-1α in the navigation of entorhinal axons. We examined the distribution of SDF-1α and its receptor, CXCR4, in the hippocampus and EC specimens obtained from rats on postnatal day 0. Axial sections of the hippocampus and EC were immunostained with the anti-SDF-1 or anti-CXCR4 antibody. Intense immunoreactivity for SDF-1 was detected in the dentate granule neurons labeled with the anti-NeuN antibody (Fig. 2*A*,*B*). The signal yielded by SDF-1α disappeared when the antibody against SDF-1α was preincubated with excess of recombinant SDF-1α (2.5 μg) (Fig. 2*C*). Preincubation of the anti-NeuN antibody with 2.5 μg of SDF-1α had no effects on the signals yielded by NeuN

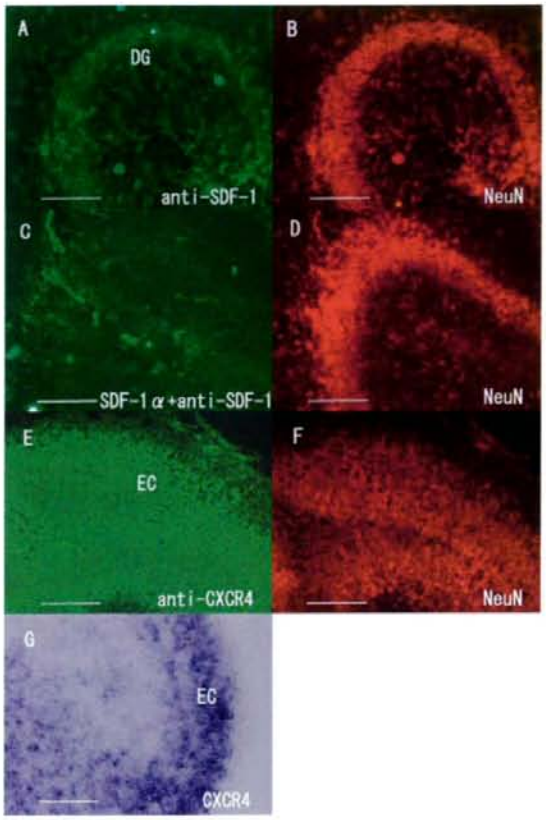

Figure 2. Distribution of stromal cell-derived factor 1α in the DG and of its receptor, CXCR4, in the EC. ***A***, ***B***, Axial sections of the DG obtained from rats at postnatal days 0–1 were immunostained with the anti-SDF-1α (***A***) and anti-NeuN antibodies (***B***). Double immunostaining with these antibodies demonstrated that SDF-1α is expressed in the granule neurons in the DG. ***C***, ***D***, A pilot experiment was performed to determine the specificity of the antibody to SDF-1α, and the absorption of the anti-SDF-1 antibody on preincubation with excess of SDF-1α was determined. ***C***, The immunoreactivity for SDF-1α in the DG disappeared. ***D***, The immunoreactivity for NeuN in the DG was maintained. ***E***, ***F***, Axial sections of the EC were stained with the anti-CXCR4 (***E***) and anti-NeuN antibodies (***F***). Double immunostaining with these antibodies demonstrated that CXCR4 is expressed in the EC neurons. ***G***, *In situ* hybridization for the detection of CXCR4 mRNA was performed in the axial section of the EC. Scale bars, 200 μm.

(Fig. 2*D*). Thus, the immunoreactivity for SDF-1α was proven to be specific.

Next, we assessed whether entorhinal neurons express the SDF-1α receptor. Immunohistochemical analysis was performed for axial sections of the EC by using the anti-CXCR4 and anti-NeuN antibodies. Colocalization of the immunoreactivity for CXCR4 and NeuN was observed in the EC cells (Fig. 2*E*,*F*). We performed *in situ* hybridization to confirm CXCR4 expression in the EC cells. The result demonstrated that CXCR4 mRNA expression was abundantly observed in the EC cells (Fig. 2*G*). Thus, CXCR4 is expressed in the EC. These results suggest that SDF-1α, which is expressed in the neurons in the DG, may act on entorhinal neurons expressing CXCR4.

SDF-1α promoted neurite growth in the dissociated entorhinal cortical neurons

Furthermore, we hypothesized that SDF-1α may play a role in the axonal elongation of entorhinal neurons. To assess this, we ex-

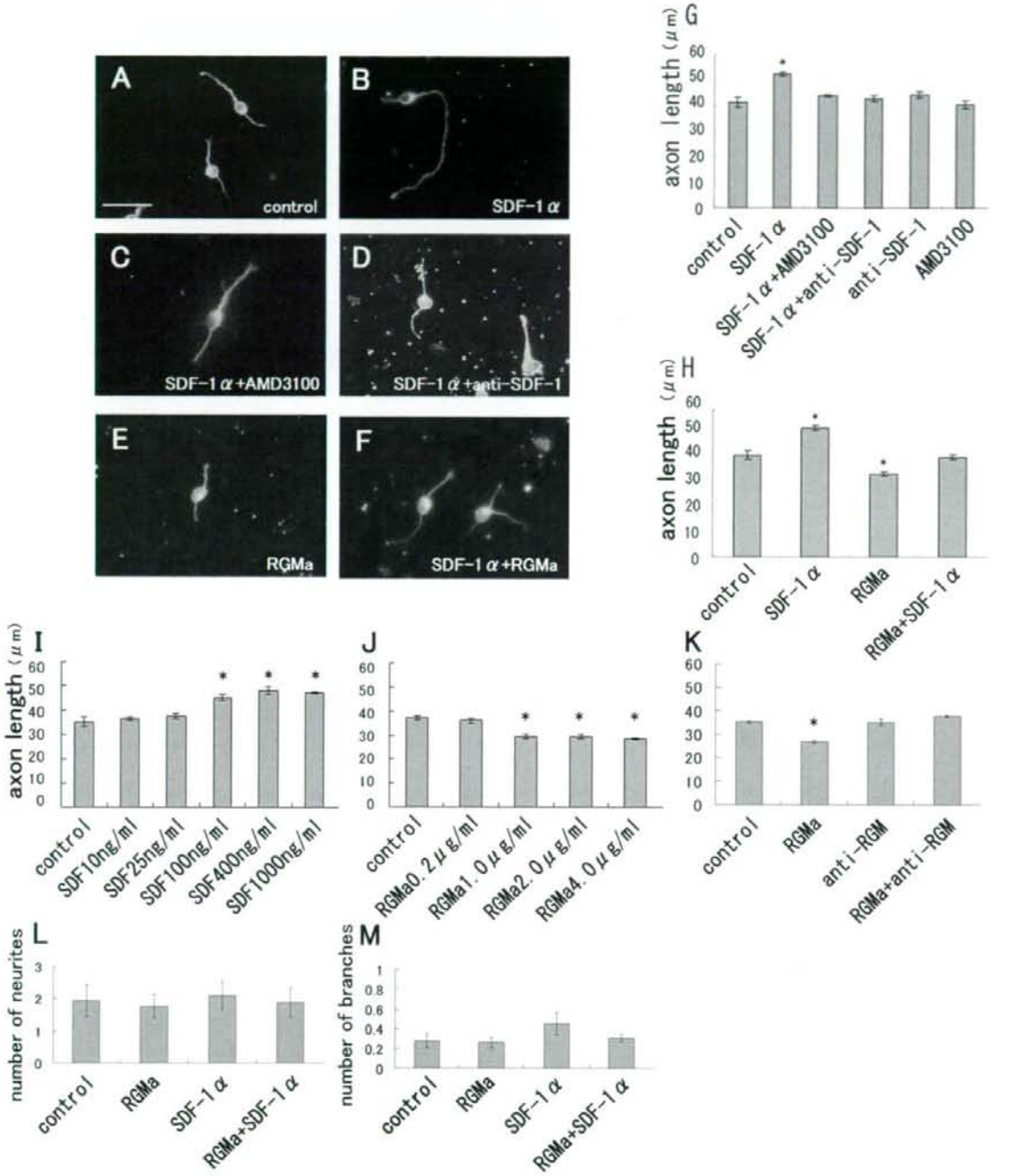

Figure 3. SDF-1α promotes neurite elongation in entorhinal cortical neurons *in vitro*. The EC neurons obtained from rats at postnatal day 0 were cultured in the absence (***A***) or presence of 400 ng/ml SDF-1α (***B–D***, ***F***). The neurons were stained with the mouse monoclonal anti-Tuj1 antibody. ***A***, ***B***, SDF-1α (400 ng/ml) promoted neurite growth in the EC neurons. ***C***, Coincubation with 400 ng/ml SDF-1α and 15 μg/ml AMD3100 (CXCR4 antagonist). ***D***, Coincubation with SDF-1α and 60 μg/ml anti-SDF-1 antibody. ***E***, RGMa (1 μg/ml) inhibited neurite growth. Scale bars, 25 μm. ***G***, Mean length of the longest neurite per neuron. AMD3100 as well as the anti-SDF-1 antibody abolished the effects of SDF-1α, although neither of these exerted any effects on neurite growth. ***H***, Coincubation with 1 μg/ml RGMa and 400 ng/ml SDF-1α resulted in the elimination of the effects of SDF-1α. The data are represented as the mean ± SEM of four independent experiments (***G***, ***H***). The asterisks (*) indicate statistical significance ($p < 0.05$) (one-way ANOVA followed by Scheffé's multiple-comparison test). ***I***, ***J***, The effects of SDF-1α (***I***) and RGMa (***J***) on neurite growth at the indicated concentrations. ***K***, The anti-RGMa antibody attenuated the neurite growth inhibition by RGMa. ***L***, The number of neurites per neuron. RGMa or SDF-1α does not alter the number of neurites significantly. ***M***, The number of branches per neuron. The data are represented as the mean ± SEM of four independent experiments (***I–M***). The asterisks (*) indicate statistical significance ($p < 0.01$) compared with the control (one-way ANOVA followed by Scheffé's multiple-comparison test).

amined the effects of SDF-1α on the neurite growth of entorhinal cortical neurons *in vitro*. The dissociated entorhinal cortical neurons isolated from rats at postnatal days 0–1 were either left untreated or treated with recombinant SDF-1α at a concentration of 400 ng/ml for 24 h, fixed, and immunostained with the TuJ1 antibody. The neurite length was then measured; the average neurite length was significantly greater in the SDF-1α-treated group than in the control group (Fig. 3*A*,*B*,*G*). Furthermore, to determine whether this effect of SDF-1α was dependent on SDF-1α and its receptor, CXCR4, we used AMD3100, which is a specific SDF-1 receptor antagonist, and a neutralizing antibody against SDF-1α. The effect of SDF-1α was completely abolished if the neurons were coincubated with AMD3100 (15 μg/ml) (Fig. 3*C*,*G*) or the anti-SDF-1 antibody (60 μg/ml) (Fig. 3*D*,*G*), although AMD3100 or the anti-SDF-1 antibody did not independently exert any modulating effects on neurite elongation (Fig. 3*G*). The neurite-promoting effect of SDF-1α was found at concentrations ranging from 100 to 1000 ng/ml (Fig. 3*I*). However, SDF-1α did not significantly change the number of neurites or branches per neuron (Fig. 3*L*,*M*). These results strongly suggest that SDF-1α promotes neurite growth in the entorhinal cortical neurons via its receptor CXCR4.

Stripe and outgrowth assays performed in a previous study revealed that entorhinal axons are repelled by RGMa (Brinks et al., 2004); this prompted us to examine the possible conflicting effects of SDF-1α and RGMa in our culture system. As expected, neurite growth in the entorhinal cortical neurons was significantly inhibited by RGMa (1–4 μg/ml) (Fig. 3*E*,*H*,*J*). The effects of SDF-1α (400 ng/ml) as well as RGMa (1 μg/ml) on neurite growth disappeared when the neurons were coincubated with both these molecules (Fig. 3*F*,*H*). In addition, the anti-RGM antibody neutralized the effect of the RGMa (Fig. 3*K*). These results support our notion that SDF-1α promotes, whereas RGMa inhibits, the neurite elongation of entorhinal neurons *in vitro*, which suggest the possibility that SDF-1α may be involved in navigating the entorhinal neurons toward the DG.

SDF-1α promotes neurite growth by a mechanism dependent on mDia1

We further explored the signaling pathway leading to the promotion of neurite growth by SDF-1α. It was previously demonstrated that mDia1 was involved in the signals downstream of SDF-1α, using cerebellar granule neurons (Arakawa et al., 2003). Thus, we assessed whether mDia1 was necessary for the effect of SDF-1α using the RNA interference technique. The entorhinal cortical neurons were transfected with mDia1 siRNA or the control siRNAs, and the expression of mDia1 was determined by Western blot analysis (Fig. 4*A*). The result demonstrated that mDia1 expression was decreased specifically at 1 or 2 d after the mDia1 siRNA transfection.

One day after the siRNA transfection, we treated the neurons with 400 ng/ml SDF-1α and incubated them for an additional 24 h. The neurite-promoting effect of SDF-1α was absent in the neurons transfected with mDia1 siRNA, but not with those transfected with the control siRNAs (Fig. 4*B*). However, Y-27632 (50 μM), the Rho kinase inhibitor, did not modulate the effect of SDF-1α (Fig. 4*B*). These results strongly suggest that SDF-1α promotes neurite growth by a mechanism dependent on mDia1.

SDF-1α navigates perforant fibers from the EC to the DG

Because the above results obtained from the *in vitro* analysis suggest that SDF-1α plays a role in navigation of the axons of the EC neurons to the DG, we attempted to test this hypothesis in a more

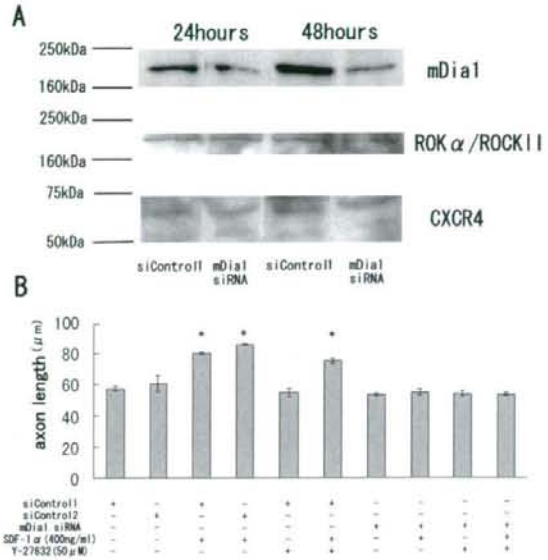

Figure 4. Neurite elongation by SDF-1α is dependent on mDia1. ***A***, The EC neurons obtained from rats at postnatal day 0 were transfected with mDia1 siRNA or control siRNA (si control). Western blot demonstrates reduction of mDia1 expression at 24 and 48 h by mDia1 siRNA. The expression of Rho kinase (ROKα) or CXCR4 was not changed by mDia1 siRNA. ***B***, Mean length of the longest neurite per neuron. The mDia1 knockdown resulted in inhibition of SDF-1α-dependent axon elongation. The data are represented as the mean ± SEM of four independent experiments. The asterisks (*) indicate statistical significance ($p < 0.05$) compared with the control (si control) (one-way ANOVA followed by Scheffé's multiple-comparison test).

direct manner. It has been reported that *CXCR4*-knock-out mice exhibit a defect in the migration of hippocampal dentate granule neurons during the embryonic stage (Bagri et al., 2002; Lu et al., 2002); thus, these mice were not appropriate for the purpose of our study. Therefore, to examine the effects of SDF-1α on axon projection from the EC to the DG, slices of the EC and hippocampus of rats at postnatal days 0–1 were cocultured. The EC specimens were obtained from GFP transgenic rats. An entorhinal cortical slice and a hippocampal slice were exactly placed to monitor the projection of the perforant fibers from the EC to the DG (Figs. 1, 5*A*), and the slices were incubated for 9 d in the absence or presence of 50 μg/ml AMD3100 or 60 μg/ml anti-SDF-1 antibody. As shown in Figure 5*A*, this coculture system facilitated distinct visualization of projection of the EC neuronal axons to the DG. The green fluorescent signals obtained in the DG reflected the fibers projecting from the EC (Fig. 5*A–C*), and these signals were specifically observed in the outer molecular layer of the DG. The green fluorescent intensities of the perforant fibers were measured and normalized to those obtained in the EC (Fig. 5*F*); the value thus obtained represented the level of neuronal projection from the EC to the DG. We then treated the explant culture with AMD3100 or the anti-SDF1 antibody. Notably, both treatments resulted in a significant reduction in the level of neuronal projection from the EC to the DG (Fig. 5*D–F*). However, this reduction was greater in the AMD3100-treated group than in the anti-SDF-1 antibody-treated group. These results suggest that SDF-1α and its receptor, CXCR4, are necessary for appropriate projection of the perforant fibers from the EC to the DG. However, because *CXCR4*-knock-out mice exhibit a defect in the migration of hippocampal dentate granule neurons during the embryonic stage, it is possible that treatment with the anti-SDF-1

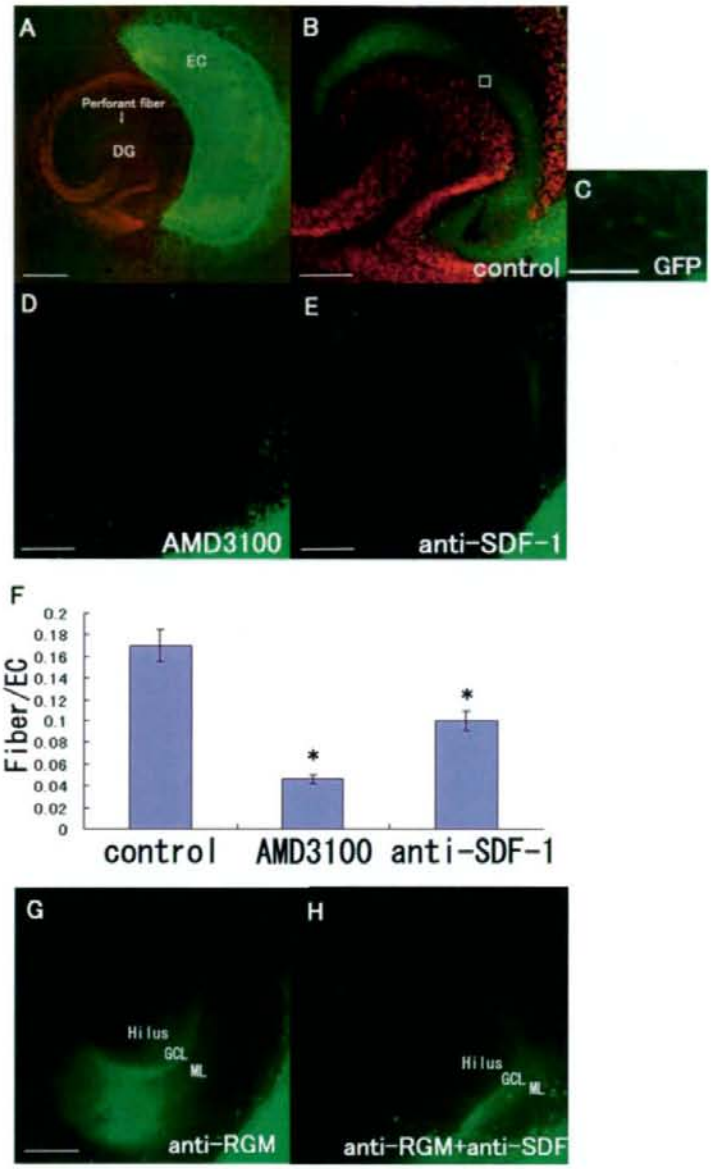

Figure 5. SDF-1α is necessary for the projection of perforant fibers from the EC to the DG. ***A***, The GFP-labeled EC (green) and DG (red; stained with anti-Prox1 antibody) slices were obtained from rats at postnatal days 0–1. ***B***, ***D***, ***E***, The tissue slices were incubated for 9 d in the absence (***B***) or presence of 50 μg/ml AMD3100 (CXCR4 antagonist) (***D***) or 60 μg/ml anti-SDF-1 antibody (***E***). ***A***, ***B***, Perforant fibers (arrow) running from the EC to the DG are visible. ***C***, High-magnification view of a square in ***B***. ***D***, ***E***, Treatment with AMD3100 (SDF-1 receptor antagonist) or the anti-SDF-1 antibody reduced the projection of the perforant fibers from the EC to the DG. ***F***, The fluorescence intensity of the perforant fibers in the DG was measured. The data are represented as the mean ± SEM of four samples (8 fields of 25 μm^2 each) of each group. The perforant fiber projection was significantly lower in the AMD3100- and anti-SDF-1 antibody-treated groups. The asterisks (*) indicate statistical significance ($p < 0.05$) (one-way ANOVA followed by Scheffé's multiple-comparison test). ***G***, ***H***, The tissue slices were incubated with anti-RGM antibody (***G***) or anti-RGM antibody and anti-SDF-1 antibody (***H***). Note the loss of the layer-specific termination of GFP-positive fibers after treatment with the anti-RGMa antibody. GCL, Granule cell layer; ML, molecular layer. Scale bars: ***A***, 500 μm; ***B***, ***D***, ***E***, ***G***, 200 μm; ***C***, 12 μm.

antibody or AMD3100 in our experimental model may have affected the migration of neurons to the DG, causing the projection of entorhinal neuronal axons to disappear. To rule out this possibility, we performed immunostaining by using the anti-Prox1 antibody, which is used for labeling dentate granule neurons (Fig. 6*A–C*). We observed that the DG structure was not disturbed after treatment with AMD3100 or the anti-SDF-1 antibody (Fig. 6*B*,*C*). Furthermore, no abnormal neuronal morphology was observed, and the number of neurons in the DG was not affected by these treatments (data not shown). These results demonstrate that blockade of the SDF-1–CXCR4 pathway for 9 d *in vitro*, beginning from postnatal days 0 and 1, does not disturb the DG structure. Thus, reduction in the perforant fiber projection on treatment with AMD3100 or the anti-SDF-1 antibody was not attributable to overall malformation of the dentate granule cell layers.

It was previously reported that disrupting the RGM function resulted in the loss of appropriate termination of the perforant fibers by using the coculture system (Brinks et al., 2004). We confirmed this result by using the neutralizing antibody to RGMa (Hata et al., 2006). After treatment with the anti-RGMa antibody, the perforant fiber projection was found diffusely in the DG (Fig. 5*G*), demonstrating inappropriate hippocampal projection. When we treated the coculture with the anti-RGMa and anti-SDF-1 antibodies simultaneously, signal intensity for the perforant fiber projection decreased compared with that of the anti-RGMa antibody treatment (Fig. 5*G*,*H*). This may be attributable to the combined effect of the loss of projection by the anti-SDF-1 antibody and inappropriate projection by the anti-RGMa antibody.

Appropriately projecting neurons form synapses with the target neurons; therefore, we assessed synapse formation between the perforant fibers and the dentate granule neurons. The hippocampal slices were cultured in contact with or in the absence of EC slices and were immunostained with the anti-PSD-95 antibody that labels postsynaptic densities on dendritic spines and with the anti-Prox1 antibody that labels granule cell layers (Fig. 7*A*,*B*). PSD-95-positive dots were observed in the border regions of the perforant fibers and the DG (Fig. 7*A*, square; *C*). The fluorescent dots labeled with the anti-PSD-95 antibody were counted in five different fields (each with a 100 μm^2 area) for each sample ($n = 4$), and the average number of dots was calculated (Fig. 7*G*). When the hippocampal slice was cultured in the absence of the EC slice, the number of PSD-95-positive dots (Fig. 7*D*,*G*) observed decreased considerably compared with the number observed when the control culture comprising the EC and DG was used (Fig. 7*C*,*G*). Thus, the re-

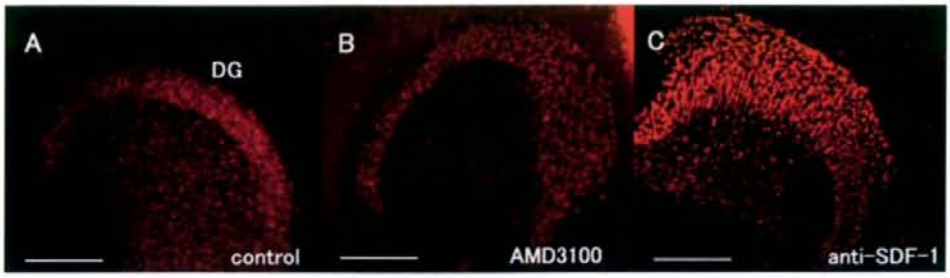

Figure 6. Treatment with AMD3100 or the anti-SDF-1 antibody does not disturb the DG structure. ***A–C***, Tissue slices of the EC and DG obtained from rats at postnatal days 0–1 were incubated for 9 d in the absence (***A***) (control) or presence of 50 μg/ml AMD3100 (***B***) or 60 μg/ml anti-SDF-1 antibody (***C***). The tissues were immunostained with the anti-Prox1 antibody. The structure of the dentate granule cell layers was maintained in all the groups. Thus, the reduced projection of the perforant fibers on treatment with AMD3100 or the anti-SDF-1 antibody was not attributable to the overall disturbance of the dentate granule cell layers. Scale bars, 200 μm.

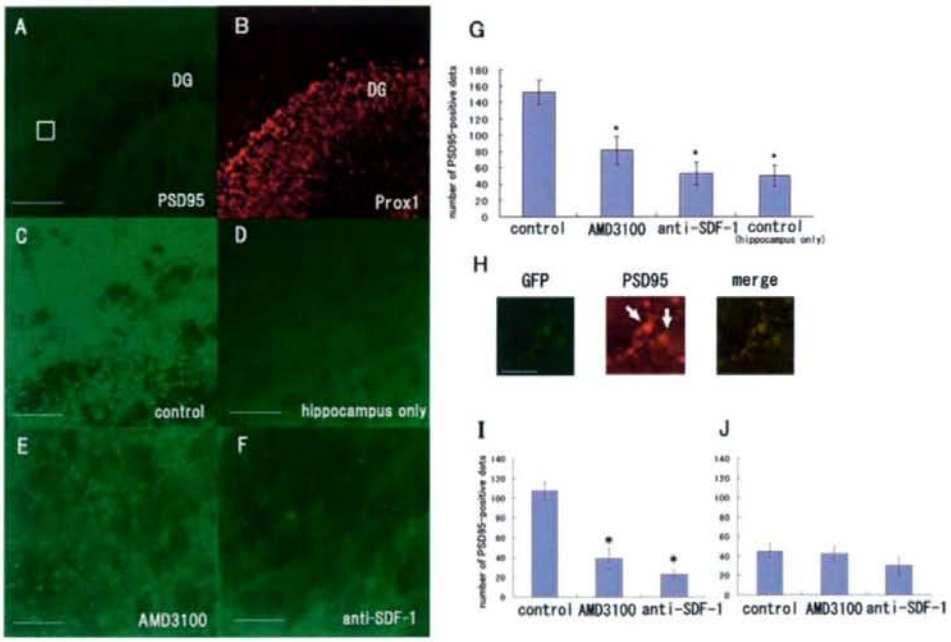

Figure 7. SDF-1α is necessary for synapse formation between the perforant fibers and the DG neurons. ***A***, Slices of the EC and hippocampus were obtained from the rats at postnatal days 0–1 and were incubated for 9 d in the absence (***A–C***) or presence of 50 μg/ml AMD3100 (***E***) or 60 μg/ml anti-SDF-1 antibody (***F***). ***D***, The hippocampal slices were cultured in the absence of the EC slices. The tissues were stained with the anti-PSD95 (green) and anti-Prox1 antibodies (red). ***C***, PSD-95-positive signals were observed between the perforant fibers and the DG. ***D***, The PSD-95-positive signals were considerably fewer in the hippocampal slices cultured in the absence of EC slices than in the coculture of the EC and hippocampus. ***E***, ***F***, Treatment with AMD3100 or the anti-SDF-1 antibody resulted in a decrease in the number of PSD-95-positive signals. ***G***, The number of PSD-95-positive signals in the DG was measured and quantified. ***H***, The hippocampal slices were obtained from wild-type rats and the EC slices were from GFP transgenic rats. The tissues were stained with the anti-PSD95 (red) and anti-GFP antibodies (green). The PSD-95-positive signals contacted with the GFP-positive perforant fibers. ***I***, The number of PSD-95-positive signals that contacted with the perforant fibers was measured and quantified. ***J***, The number of PSD-95-positive signals that did not contact with the perforant fibers was measured and quantified. ***G***, ***I***, ***J***, The data are represented as the mean ± SEM of four samples of each group (5 different fields of 100 μm^2 area for each sample). The asterisks (*) indicate statistical significance ($p < 0.05$) (two-way ANOVA followed by Scheffé's multiple-comparison test). Scale bars: ***A***, ***B***, 100 μm; ***C–F***, 25 μm; ***H***, 12 μm.

duced number of PSD-positive dots observed reflected synapses formed between the entorhinal and DG neurons. The PSD-95-positive dots observed in the case of the coculture of the hippocampal and EC slices treated with AMD3100 or the anti-SDF-1 antibody were significantly fewer than those observed in the case of the control group (Fig. 7*C*,*E–G*). To directly assess whether the decrease in synaptic density by the blockade of SDF-1 signaling is a consequence of reduction in the density of perforant fibers or a decrease in the density of synapses adjacent to perforant fibers, we performed simultaneous immunohistochemical analyses for PSD-95 and GFP. The PSD-95-positive dots contacted with the GFP-positive perforant fibers (Fig. 7*H*). We obtained consistent results when the number of PSD-95-positive dots contacted with the perforant fibers was counted (Fig. 7*I*). The number of the PSD-95-positive signals that did not contact with the perforant fibers was not significantly changed by either treatment (Fig. 7*J*). These results strongly support the notion that synapse formation between the perforant fibers and DG neurons depends on SDF-1α and its receptor.

Finally, we attempted to confirm that the perforant fibers pro-

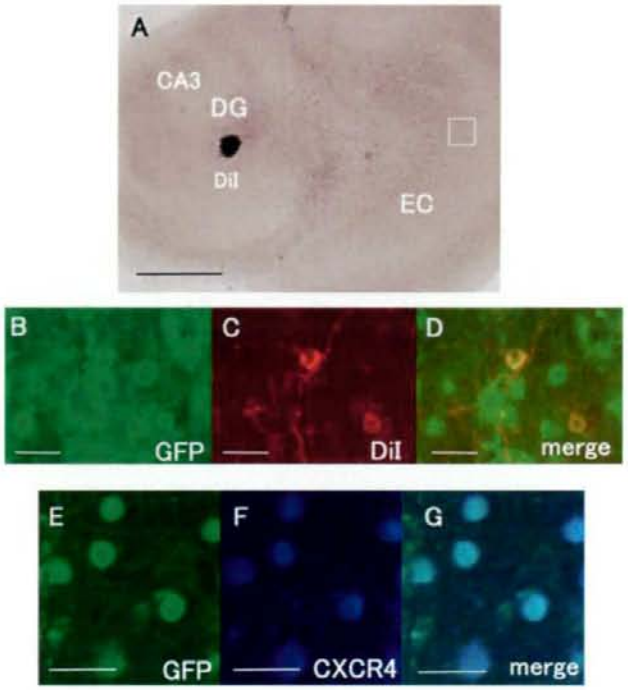

Figure 8. The EC neurons that project into the DG express CXCR4. ***A***, DiI was placed into the DG to label the perforant fibers. ***B–D***, The GFP signals in the EC were colocalized with those of DiI. ***E–G***, The immunoreactivity for CXCR4 (blue) is observed in the GFP-positive cells in the EC. Scale bars: ***A***, 500 μm; ***B–G***, 20 μm.

jecting to the DG expressed CXCR4. The cocultures were subjected to retrograde labeling of the perforant fibers projecting to the DG by DiI (Fig. 8*A*). The fibers and the neurons in the EC (Fig. 8*B–D*), which were labeled by DiI, were GFP-positive. The GFP-positive entorhinal neurons were immunoreactive for CXCR4 (Fig. 8*E–G*). Thus, these results demonstrate that the perforant fibers expressed the receptor for SDF-1α.

Discussion

The chemokine SDF-1α and its receptor, CXCR4, are known to play important roles in neural development (Tran and Miller, 2003). The present study unveiled several features of SDF-1α and CXCR4 during the early developmental stage of the hippocampus. First, the histochemical analysis revealed that SDF-1α is distributed in the DG neurons and that CXCR4 is expressed in the EC neurons of rats at postnatal day 0. Consistent with this observation, previous studies have reported that SDF-1α mRNAs are expressed in the granule cell layer of the DG in the brains of early postnatal rats (Tham et al., 2001; Berger et al., 2007). These data prompted us to hypothesize that SDF-1α expression in the DG induces axonal elongation of EC neurons expressing CXCR4.

SDF-1α promotes the neurite growth of dissociated EC neurons, and the neutralizing anti-SDF-1 antibody as well as AMD3100, a CXCR4 antagonist, abolishes this effect of SDF-1α. Because previous studies have demonstrated that SDF-1α promotes axonal elongation and the branching of hippocampal neurons (Arakawa et al., 2003; Pujol et al., 2005; Pritchett et al., 2007), SDF-1α distributed in the hippocampus may have multiple roles during neural development. Although, in the present study, the neurite growth assay for 24 h revealed that the number of branches or neurites was not significantly altered by SDF-1α, a longer assay time may be required to draw a conclusion. However, RGMa compels the entorhinal fibers to remain within their appropriate target zone (Brinks et al., 2004). Because our study shows that RGMa and SDF-1α exert opposing effects on the neurite growth of the EC neurons *in vitro*, conflicting signals elicited by these molecules are suggested to contribute to appropriate targeting of the perforant fibers. Thus, the ratio of the concentration of these factors in a local environment might determine the elongation, retraction, or termination of the perforant fibers. Interestingly, a previous report has demonstrated that SDF-1α reduces the repellent action of Slit-2 on retinal ganglion neurons; semaphorin 3A, on dorsal root ganglion neurons; and semaphorin 3C, on sympathetic neurons (Chalasani et al., 2003). However, these researchers did not observe the axon-promoting effects of SDF-1α on these neurons (retinal ganglion neurons, dorsal root ganglion sensory neurons, and sympathetic neurons) (Chalasani et al., 2003).

In the present study, we explored the signaling mechanism of axon elongation induced by SDF-1α. Facilitation of axon elongation of the cerebellar granule neurons by a low concentration of SDF-1α (100 and 250 ng/ml) was previously reported (Arakawa et al., 2003). This effect of axon elongation disappeared if the cells were treated with higher concentrations (500 and 1000 ng/ml) of SDF-1α (Arakawa et al., 2003), whereas our study revealed that SDF-1α at a concentration of 100–1000 ng/ml promoted neurite growth of the EC neurons. Consistent with the previous observation (Arakawa et al., 2003), the mDia1 pathway but not Rho kinase activation, is required for the promotion of neurite elongation in our study. Thus, our results support the critical role of the SDF-1α/mDia1 pathway in mediating axon elongation of the EC neurons.

The expression profiles of SDF-1α and CXCR4 and the axon-promoting effects of the former on dissociated entorhinal cortical neurons prompted us to assume that SDF-1α induces the projection of the perforant fibers from the EC to DG. However, because the structures of the DG as well as the cerebral cortex are destroyed in *CXCR4*-knock-out mice (Bagri et al., 2002; Lu et al., 2002; Paredes et al., 2006; Li et al., 2008), *CXCR4*- or *SDF-1*-knock-out mice were not appropriate for this analysis. To overcome this difficulty, we used entorhino-hippocampal slice cultures prepared from rats at postnatal days 0–1, in whom the dentate granule layers are almost established (Schlessinger et al., 1975; Altman and Bayer, 1990). A merit of this system is that the DG and cortical structures are not disturbed by blockade of the SDF-1–CXCR4 pathway. In addition, this coculture system enabled us to easily examine the molecular pathways by using specific inhibitors and neutralizing antibodies. With this slice culture system, we observed, for the first time, that blockade of the SDF-1–CXCR4 pathway reduced the projection of perforant fibers, as visualized via GFP signals; this strongly suggests that

SDF-1α promotes the growth of perforant fibers. Consistent with this observation, SDF-1α induces axonal elongation in cultured cerebellar granule neurons (Arakawa et al., 2003), and SDF-1α antagonizes the repellent effects of Slit/Robo signaling in the visual system (Chalasani et al., 2007). Therefore, it is suggested that SDF-1α is involved in promoting axonal growth in several types of neurons. Conversely, RGMa appears to restrict entorhinal fibers to their correct layer of the DG (Brinks et al., 2004). We confirmed this observation (Fig. 5*G*,*H*), and found that inhibition of both RGMa and SDF-1α resulted in reduction of the correct target axons from the EC. Therefore, SDF-1α and RGMa play important roles in correct navigation of the perforant fibers to the outer molecular layer of the DG. Concerning the signal transduction mechanism, we previously demonstrated that RGMa inhibits neurite growth by activating RhoA and Rho kinase (Hata et al., 2006). Because SDF-1α promotes neurite growth, which requires mDia1 (Fig. 4*B*), mDia1 and RhoA/Rho kinase pathways may be involved in appropriate termination of the perforant fibers, which requires elongation and termination of the axons.

PSD-95 belongs to a family of membrane-associated proteins found in the postsynaptic densities of neurons (Kornau et al., 1995; Nam and Chen, 2005). PSD-95 functions to recruit signaling components at the synapse (Kim and Sheng, 2004) and promotes the maturation of dendritic spines (El-Husseini et al., 2000; Charych et al., 2006). We detected PSD-95 immunoreactivity in the areas of contact between the dentate granule neurons and the perforant fibers. Because the number of PSD-95-positive particles on the perforant fibers was reduced when the SDF-1–CXCR4 pathway was blocked, this pathway may be associated with postsynaptic maturation of the perforant fibers and dentate granule neurons.

In conclusion, the present study identified a new molecule that promotes the axonal elongation of perforant fibers from the EC to the DG neurons. In the future, it would be interesting to determine whether a deficit in neural wiring can cause abnormal brain function.

References

Altman J, Bayer SA (1990) Migration and distribution of two populations of hippocampal granule cell precursors during the perinatal and postnatal periods. J Comp Neurol 301:365–381.

Ara T, Tokoyoda K, Okamoto R, Koni PA, Nagasawa T (2005) The role of CXCL12 in the organ-specific process of artery formation. Blood 105:3155–3161.

Arakawa Y, Bito H, Furuyashiki T, Tsuji T, Takemoto-Kimura S, Kimura K, Nozaki K, Hashimoto N, Narumiya S (2003) Control of axon elongation via an SDF-1alpha/Rho/mDia pathway in cultured cerebellar granule neurons. J Cell Biol 161:381–391.

Bagri A, Gurney T, He X, Zou YR, Littman DR, Tessier-Lavigne M, Pleasure SJ (2002) The chemokine SDF1 regulates migration of dentate granule cells. Development 129:4249–4260.

Belmadani A, Tran PB, Ren D, Assimacopoulos S, Grove EA, Miller RJ (2005) The chemokine stromal cell-derived factor-1 regulates the migration of sensory neuron progenitors. J Neurosci 25:3995–4003.

Berger O, Li G, Han SM, Paredes M, Pleasure SJ (2007) Expression of SDF-1 and CXCR4 during reorganization of the postnatal dentate gyrus. Dev Neurosci 29:48–58.

Bleul CC, Wu L, Hoxie JA, Springer TA, Mackay CR (1997) The HIV coreceptors CXCR4 and CCR5 are differentially expressed and regulated on human T lymphocytes. Proc Natl Acad Sci U S A 94:1925–1930.

Brinks H, Conrad S, Vogt J, Oldekamp J, Sierra A, Deitinghoff L, Bechmann I, Alvarez-Bolado G, Heimrich B, Monnier PP, Mueller BK, Skutella T (2004) The repulsive guidance molecule RGMa is involved in the formation of afferent connections in the dentate gyrus. J Neurosci 24:3862–3869.

Chalasani SH, Sabelko KA, Sunshine MJ, Littman DR, Raper JA (2003) A chemokine, SDF-1, reduces the effectiveness of multiple axonal repellents and is required for normal axon pathfinding. J Neurosci 23:1360–1371.

Chalasani SH, Sabol A, Xu H, Gyda MA, Rasband K, Granato M, Chien CB, Raper JA (2007) Stromal cell-derived factor-1 antagonizes slit/robo signaling *in vivo*. J Neurosci 27:973–980.

Charych EI, Akum BF, Goldberg JS, Jörnsten RJ, Rongo C, Zheng JQ, Firestein BL (2006) Activity-independent regulation of dendrite patterning by postsynaptic density protein PSD-95. J Neurosci 26:10164–10176.

Chen H, Bagri A, Zupicich JA, Zou Y, Stoeckli E, Pleasure SJ, Lowenstein DH, Skarnes WC, Chédotal A, Tessier-Lavigne M (2000) Neuropilin-2 regulates the development of selective cranial and sensory nerves and hippocampal mossy fiber projections. Neuron 25:43–56.

Cheng HJ, Bagri A, Yaron A, Stein E, Pleasure SJ, Tessier-Lavigne M (2001) Plexin-A3 mediates semaphorin signaling and regulates the development of hippocampal axonal projections. Neuron 32:249–263.

El-Husseini AE, Schnell E, Chetkovich DM, Nicoll RA, Bredt DS (2000) PSD-95 involvement in maturation of excitatory synapses. Science 290:1364–1368.

Gu C, Rodriguez ER, Reimert DV, Shu T, Fritzsch B, Richards LJ, Kolodkin AL, Ginty DD (2003) Neuropilin-1 conveys semaphorin and VEGF signaling during neural and cardiovascular development. Dev Cell 5:45–57.

Hata K, Fujitani M, Yasuda Y, Doya H, Saito T, Yamagishi S, Mueller BK, Yamashita T (2006) RGMa inhibition promotes axonal growth and recovery after spinal cord injury. J Cell Biol 173:47–58.

Kim E, Sheng M (2004) PDZ domain proteins of synapses. Nat Rev Neurosci 5:771–781.

Kornau HC, Schenker LT, Kennedy MB, Seeburg PH (1995) Domain interaction between NMDA receptor subunits and the postsynaptic density protein PSD-95. Science 269:1737–1740.

Koyama R, Yamada MK, Nishiyama N, Matsuki N, Ikegaya Y (2004a) Developmental switch in axon guidance modes of hippocampal mossy fibers *in vitro*. Dev Biol 267:29–42.

Koyama R, Yamada MK, Fujisawa S, Katoh-Semba R, Matsuki N, Ikegaya Y (2004b) Brain-derived neurotrophic factor induces hyperexcitable reentrant circuits in the dentate gyrus. J Neurosci 24:7215–7224.

Li G, Adesnik H, Li J, Long J, Nicoll RA, Rubenstein JL, Pleasure SJ (2008) Regional distribution of cortical interneurons and development of inhibitory tone are regulated by Cxcl12/Cxcr4 signaling. J Neurosci 28:1085–1098.

Lieberam I, Agalliu D, Nagasawa T, Ericson J, Jessell TM (2005) A Cxcl12-CXCR4 chemokine signaling pathway defines the initial trajectory of mammalian motor axons. Neuron 47:667–679.

Lu M, Grove EA, Miller RJ (2002) Abnormal development of the hippocampal dentate gyrus in mice lacking the CXCR4 chemokine receptor. Proc Natl Acad Sci U S A 99:7090–7095.

Ma Q, Jones D, Borghesani PR, Segal RA, Nagasawa T, Kishimoto T, Bronson RT, Springer TA (1998) Impaired B-lymphopoiesis, myelopoiesis, and derailed cerebellar neuron migration in CXCR4- and SDF-1-deficient mice. Proc Natl Acad Sci U S A 95:9448–9453.

Nam CI, Chen L (2005) Postsynaptic assembly induced by neurexin-neuroligin interaction and neurotransmitter. Proc Natl Acad Sci U S A 102:6137–6142.

Nguyen Ba-Charvet KT, Brose K, Marillat V, Kidd T, Goodman CS, Tessier-Lavigne M, Sotelo C, Chédotal A (1999) Slit2-Mediated chemorepulsion and collapse of developing forebrain axons. Neuron 22:463–473.

Okabe M, Ikawa M, Kominami K, Nakanishi T, Nishimune Y (1997) "Green mice" as a source of ubiquitous green cells. FEBS Lett 407:313–319.

Paredes MF, Li G, Berger O, Baraban SC, Pleasure SJ (2006) Stromal-derived factor-1 (CXCL12) regulates laminar position of Cajal-Retzius cells in normal and dysplastic brains. J Neurosci 26:9404–9412.

Pritchett J, Wright C, Zeef L, Nadarajah B (2007) Stromal derived factor-1 exerts differential regulation on distinct cortical cell populations in vitro. BMC Dev Biol 7:31.

Pujol F, Kitabgi P, Boudin H (2005) The chemokine SDF-1 differentially regulates axonal elongation and branching in hippocampal neurons. J Cell Sci 118:1071–1080.

Schlessinger AR, Cowan WM, Gottlieb DI (1975) An autoradiographic study of the time of origin and the pattern of granule cell migration in the dentate gyrus of the rat. J Comp Neurol 159:149–175.

Shimogori T, VanSant J, Paik E, Grove EA (2004) Members of the Wnt, Fz,

and Frp gene families expressed in postnatal mouse cerebral cortex. J Comp Neurol 473:496–510.

Skutella T, Nitsch R (2001) New molecules for hippocampal development. Trends Neurosci 24:107–113.

Stein E, Savaskan NE, Ninnemann O, Nitsch R, Zhou R, Skutella T (1999) A role for the Eph ligand ephrin-A3 in entorhino-hippocampal axon targeting. J Neurosci 19:8885–8893.

Steup A, Lohrum M, Hamscho N, Savaskan NE, Ninnemann O, Nitsch R, Fujisawa H, Püschel AW, Skutella T (2000) Sema3C and netrin-1 differentially affect axon growth in the hippocampal formation. Mol Cell Neurosci 15:141–155.

Stumm R, Höllt V (2007) CXC chemokine receptor 4 regulates neuronal migration and axonal pathfinding in the developing nervous system: implications for neuronal regeneration in the adult brain. J Mol Endocrinol 38:377–382.

Tham TN, Lazarini F, Franceschini IA, Lachapelle F, Amara A, Dubois-Dalcq M (2001) Developmental pattern of expression of the alpha chemokine stromal cell-derived factor 1 in the rat central nervous system. Eur J Neurosci 13:845–856.

Tran PB, Miller RJ (2003) Chemokine receptors in the brain: a developing story. J Comp Neurol 457:1–6.

Vilz TO, Moepps B, Engele J, Molly S, Littman DR, Schilling K (2005) The SDF-1/CXCR4 pathway and the development of the cerebellar system. Eur J Neurosci 22:1831–1839.

Zhao S, Förster E, Chai X, Frotscher M (2003) Different signals control laminar specificity of commissural and entorhinal fibers to the dentate gyrus. J Neurosci 23:7351–7357.

Zou YR, Kottmann AH, Kuroda M, Taniuchi I, Littman DR (1998) Function of the chemokine receptor CXCR4 in haematopoiesis and in cerebellar development. Nature 393:595–599.

Neuroradiology (2008) 50:605–611
DOI 10.1007/s00234-008-0379-5

FUNCTIONAL NEURORADIOLOGY

Cerebral white matter damage in frontotemporal dementia assessed by diffusion tensor tractography

Koushun Matsuo · Toshiki Mizuno · Kei Yamada · Kentaro Akazawa · Takashi Kasai · Masaki Kondo · Satoru Mori · Tsunehiko Nishimura · Masanori Nakagawa

Received: 28 November 2007 / Accepted: 26 February 2008 / Published online: 1 April 2008

Abstract
Introduction We used diffusion tensor imaging (DTI) to study white matter integrity in patients with frontotemporal dementia (FTD).
Methods The subjects comprised 20 patients (9 men, 11 women) with FTD and 17 age-matched healthy controls (9 men, 8 women). Based on the data obtained from DTI, we performed tractography of the major cerebral pathways, including the pyramidal tracts, genu and splenium of the corpus callosum (CC), bilateral arcuate fasciculi (AF), inferior longitudinal fasciculi (ILF) and uncinate fasciculi (UF). We measured the values of fractional anisotropy (FA) in each fiber and statistically compared the findings in patients with those in controls.
Results We found a significant decrease in FA values in the selected association fibers as well as anterior fibers of the CC in the patients with FTD. The greatest decrease in mean FA of the UF was seen in advanced FTD. On the other hand, there were no significant differences in FA in the bilateral pyramidal tracts.
Conclusion The features of FTD from the view point of cerebral white matter damage were revealed by tractography based on DTI. DTI is therefore considered to be a useful method, and may provide clues to elucidating the pathogenesis of FTD.

Keywords Frontotemporal dementia (FTD) · Diffusion tensor imaging (DTI) · Tractography · Cerebral white matter (CWM) damage · Fractional anisotropy (FA)

K. Matsuo · T. Mizuno (✉) · T. Kasai · M. Kondo · M. Nakagawa
Department of Neurology, Graduate School of Medical Science, Kyoto Prefectural University of Medicine,
Kajiicho 465, Hirokoji-Kawaramachi dori, Kamigyo-ku,
Kyoto 602-8566, Japan
e-mail: mizuno@koto.kpu-m.ac.jp

K. Yamada · K. Akazawa · T. Nishimura
Department of Radiology, Graduate School of Medical Science, Kyoto Prefectural University of Medicine,
Kyoto, Japan

S. Mori
Department of Neurology, Matsushita Memorial Hospital,
Osaka, Japan

Introduction

Frontotemporal dementia (FTD) is the third most common clinical category of cortical dementia, following Alzheimer's disease (AD) and Lewy body disease. The diagnostic criteria for FTD were initially proposed by the Lund and Manchester Groups [1]. The concept of FTD was later expanded and roughly classified into two major subtypes: frontal variant FTD (fvFTD) and temporal variant FTD (tvFTD). The former is clinically characterized by progressive change in personality and abnormal behavior, and the latter by the presence of progressive aphasia or deficits in semantic knowledge [2].

The most characteristic macroscopic brain feature of FTD is localized atrophy involving the frontal and/or temporal lobes. Microscopically, FTD is characterized by substantial gliosis in the white matter as well as neuronal loss [3–5]. A recent study that attempted to quantify the histological changes in FTD revealed significantly more astrocytes and microglia in the frontal cortices compared with controls [6]. Conventional MRI studies have revealed abnormal signal intensities in the frontal white matter lesions of patients with FTD as well as lobar atrophy [7]. However, it is difficult to assess the degree of cerebral white matter (CWM) damage in this disease in vivo directly

and quantitatively using these conventional imaging techniques. Catani et al. used proton magnetic resonance spectroscopy (^{1}H-MRS) to study in vivo the integrity of axonal fibers connecting perisylvian language areas in primary progressive aphasia (PPA) and AD, and found a marked difference in the distribution of *N*-acetylaspartate to creatine between PPA and AD [8].

Diffusion tensor imaging (DTI) is a recently developed imaging technique that provides information about tissue microstructure and its physiological state [9, 10]. Through measurements of anisotropy of the water molecular diffusion in brain tissue, DTI can now assess changes in white matter integrity, and has been applied to the study of other neurodegenerative diseases, including amyotrophic lateral sclerosis [11, 12], Parkinson's disease [13], AD [14, 15] and multiple system atrophy [16].

Studies of CWM lesions in FTD using other DTI techniques have also been reported [2, 17]. One such technique is the "region of interest" (ROI) approach [17]. This is a basic and useful method, although it has certain limitations in that identification of anatomical locations and reproducibility of measured values cannot be guaranteed without standardization. Another method is voxel-based analysis (VBA). Using this method, Borroni et al. recently reported a significant CWM reduction in FTD and showed characteristic differences between fvFTD and tvFTD [2]. Although this is an automated, unbiased and operator-independent approach, it is difficult to use for accurate analysis in some regions (e.g. around the ventricles) near areas that show extremely high or low anisotropy. If the resolution is low, misregistration will occur [18].

Data analysis based on MR tractography has recently become possible [19]. Tract-specific measurement (TSM) allows better anatomical localization of single tracts on MRI as compared to the ROI or VBA methods [18]. Its major advantage is that it allows easy identification of specific CWM fibers and the acquisition of more specific information about them. Therefore, we adopted TSM in this study as the best method.

The nerve fibers in the CWM are classified into three subtypes: projection fibers, commissural fibers and association fibers. The association fibers constructing neuronal pathways within the hemisphere (intrahemisphere) are believed to be related to higher brain functions. For example, the arcuate fasciculus (AF) connecting Broca's area with Wernicke's area plays an important role in verbal function [20]. The uncinate fasciculus (UF) connecting the frontal lobe (orbital gyri and middle frontal gyri) with the anterior temporal lobe medial site is associated with memory function [21]. The inferior longitudinal fasciculus (ILF) connecting the occipital lobe with the anterior part of the temporal lobe is involved in visual memory and emotional processing [22].

We hypothesize that the degenerative process in FTD may affect frontal connections more than other connections, and the symptom profile may correlate with damage along specific pathways. However, no studies have focused on these pathways in FTD. In this study, we used DTI to quantitatively assess CWM changes in association fibers in patients with FTD and attempted to demonstrate specific neuronal pathways that might play a major role in the disease.

Methods

Subjects

Between January 2001 and December 2006, a total of 20 patients (9 men, 11 women; average age 70.8±7.15 years) who had been diagnosed as having FTD were enrolled for this study. The clinical diagnosis was made by more than one neurologist based on the international consensus criteria for FTD [1, 23]. Based on the clinical features, they were divided into the two major clinical subtypes, fvFTD and tvFTD. All subjects underwent clinical evaluation, routine laboratory examination, ^{123}I-IMP single-photon emission tomography (SPECT), and conventional brain MRI study. Atrophy of the frontotemporal lobes was detected by conventional MRI in all patients. We evaluated neuropsychological functions by screening with the Mini-mental State Examination (MMSE). All patients were then also evaluated using the Clinical Dementia Rating (CDR) scale [24] and divided into an advanced group (CDR score 2 or 3) and an early group (CDR score 0.5 or 1). Most of the patients in the advanced group had a MMSE score of less than 20 points. The patients' clinical data and classification are summarized in Table 1.

An age-matched control group comprising 17 patients (9 men, 8 women; average age 68.2±10.85 years) was also included. All of them were outpatients referred to our hospital with nonspecific complaints such as headache and dizziness. All of these patients were later diagnosed as having no significant neurological disorders. Any suspected of having mild cognitive impairment were excluded. Informed consent was obtained from all subjects.

Exclusion criteria

We excluded patients who had a history of (1) cerebral infarction or hemorrhage, (2) head trauma, (3) cancer within the past 5 years, (4) major psychiatric disease (including drug or alcohol intoxication), (5) mental retardation, or (6) motion artifact. Patients with intracranial mass lesions on MRI were also excluded.

Table 1 Clinical data of the patients with FTD.

Patient no.	Age at presentation (years)	Sex	Age at onset (years)	Main clinical symptoms	MMSE score[a]	CDR score[b]	Clinical subtype	Notes
1	63	F	60	Aphasia	5	2	Temporal variant	Slowly progressive aphasia
2	64	F	58	Abnormal behavior, personality change	10	3	Frontal variant	
3	68	M	67	Abnormal behavior	27	0.5	Frontal variant	FTDP-17 (genetically confirmed)
4	62	F	51	Abnormal behavior	23	2	Frontal variant	
5	62	F	59	Abnormal behavior	13	2	Frontal variant	
6	74	M	69	Personality change	21	1	Frontal variant	
7	70	F	70	Decreased activity	20	1	Frontal variant	
8	65	M	60	Amnestic aphasia	26	0.5	Temporal variant	
9	71	F	68	Decreased activity	23	1	Frontal variant	
10	68	M	67	Decreased activity	28	0.5	Frontal variant	
11	82	F	67	Personality change	12	2	Frontal variant	
12	70	M	70	Abnormal behavior	23	1	Frontal variant	
13	60	F	59	Semantic dementia	22	1	Temporal variant	
14	80	M	79	Amnestic aphasia	17	2	Temporal variant	
15	83	M	83	Decreased activity	26	0.5	Frontal variant	
16	78	F	77	Forgetfulness	27	0.5	Frontal variant	Slowly progressive aphasia
17	75	M	73	Aphasia	16	2	Temporal variant	
18	79	F	79	Personality change	22	1	Frontal variant	
19	73	M	72	Aphasia	24	0.5	Temporal variant	Slowly progressive aphasia
20	67	F	60	Gait disturbance, decreased attention	11	2	Frontal variant	Motor neuron type FTD

[a] Maximum score 30 points.
[b] Clinical dementia rating scores: 0 no dementia, 0.5 questionable, 1 mild, 2 moderate, 3 severe.

MRI

DTI was performed on a 1.5-T whole-body scanner (Gyroscan Intera, Philips Medical Systems, Best, The Netherlands) using a single-shot echo-planar imaging (EPI) technique (TR 6,000 ms, TE 88 ms) with a motion-probing gradient in 15 orientations. A b value of 1000 s/mm^2 was used, and 128×53 data points were recorded using a parallel imaging technique. The resolution of the acquired images was equivalent to 128×106 pixels.

Image analysis

DWI data were transferred to an off-line computer for further analysis. Tractography was carried out using PRIDE software (Philips Medical Systems) written in Interactive Data Language (RSI, Boulder, CO), and was applied for TSM in the image analysis. With this identification of the anatomical location of neuronal fibers is easier than with VBA [18]. For preparative tractography, we set at least two representative ROIs on the ipsilateral side (for example, in order to carry out tractography of the pyramidal tract, we identified the anatomical locations of the cerebral peduncle and posterior limb of the internal capsule by diffusion-weighted MRI following the colored map of the CWM). When we detected a tract between two specific ROIs, we adopted the "AND" operation as described by Wakana et al. to impose a strong constraint in tracking results [25]. Consequently, we were able to obtain and draw three-dimensional images of the CWM based on the selected ROIs. Using a similar method, other fibers (CC, AF, UF and ILF) were also obtained. We tried to analyze the superior and inferior occipitofrontal fasciculi, but they were excluded from this study because it was difficult to identify them unequivocally in some patients and the data obtained were not useful even in those in whom they were identified.

After anatomical identification of each fiber by tractography, we measured the data for mean fractional anisotropy (FA) and ADC (apparent diffusion coefficient) values by automatic calculation. The FA is an index that

indicates the degree of diffusion anisotropy and varies from 0 (diffusion equal in all directions) to 1 (diffusion entirely unidirectional) [26].

Results

The tractography for each fiber in all of the patients with FTD and controls is shown in Fig. 1. The correlation coefficients for the FA values between two measurements (first measurement and second measurement by the same examiner) were more than 0.85 for all the subjects with FTD and the controls. This suggests that the FA measurements by the same examiner were reasonably reproducible.

The mean FA values for each measured part of patients with FTD and controls are shown in Fig. 2. The first result of interest is that the mean FA values for association fibers, including the AF, UF, and ILF, were significantly lower in the FTD patients than in the controls ($P<0.01$). Secondly, the CC fibers were analyzed to detect any changes in commissural fibers in FTD. While the mean FA value in the genu ($P<0.01$) was markedly lower than in the controls, the value for the splenium was decreased only slightly ($P<0.05$). In contrast, there was no significant difference in the mean FA values in the bilateral pyramidal tracts between the FTD patients and the controls.

Although some patients with tvFTD showed asymmetry of association fibers, no significant difference was observed between right and left in each fasciculus in the FTD patients ($P>0.05$).

There were no significant differences in the mean FA values between the FTD subgroups, i.e. the advanced group and the early group, except for the values in the left UF (advanced group 0.317±0.0611, early group 0.367±0.0328; $P<0.05$). In addition, the neuropsychological function scores (MMSE and CDR) in the patients with FTD were significantly correlated with the FA values only for the left UF ($P<0.05$). Spearman's correlation coefficient (r) for the correlation between the MMSE score and FA values in the left UF was 0.499, and between the CDR score and the FA values was 0.467.

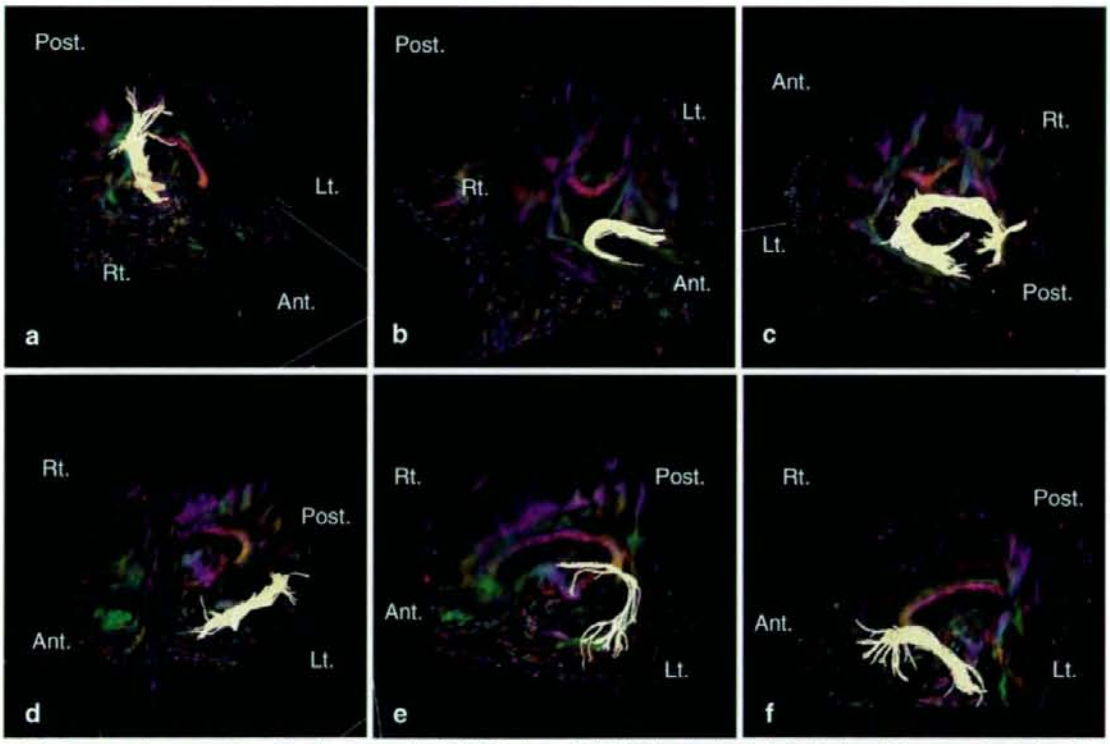

Fig. 1 Tractography was performed by three-dimensional DWI. Each tract is demonstrated as a bright yellow bundle: **a** left pyramidal tract, **b** genu of the corpus callosum, **c** splenium of the corpus callosum, **d** left inferior longitudinal fasciculus, **e** left arcuate fasciculus, **f** left uncinate fasciculus (*Ant.* anterior side, *Post.* posterior side, *Rt.* right side, *Lt.* left side)

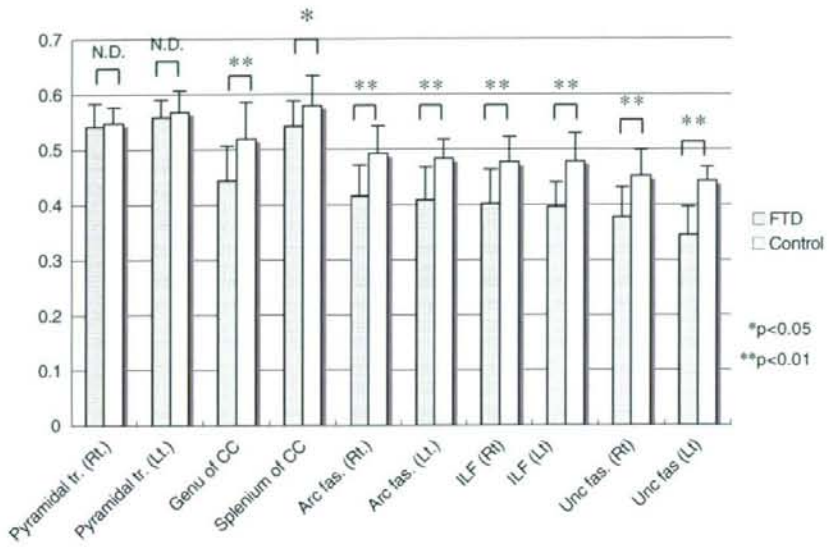

Fig. 2 Comparison of mean FA values between patients with FTD and controls. Except in the bilateral pyramidal tracts, the patients with FTD had significantly lower FA values than the controls in all of the tracts (*Rt.* right side, *Lt.* left side. *tr.* tract, *Arc fas.* arcuate fasciculus, *CC* corpus callosum, *ILF* inferior longitudinal fasciculus, *Unc fas.* uncinate fasciculus, *N.D.* not significantly different; **P*<0.05, ***P*<0.01 Mann-Whitney *U*-test)

Discussion

The neuronal fibers of the brain function as a barrier to water molecule diffusion. This barrier is the reason for the highly anisotropic diffusion observed in the white matter in comparison with the gray matter. Because water molecule diffusion is limited, the measured FA shows a relatively high value in areas with well organized and tightly packed neuronal fiber bundles, such as the cerebral peduncles, the internal capsule, and the corpus callosum [27]. If white matter structures (axons and myelin) are damaged, the diffusivity of water molecules increases, leading to less significant directionality and a decrease in the FA value. The process of white matter damage in neurodegenerative diseases is so slow that it is difficult to assess by conventional MR imaging studies, especially in the early stages. Direct measurement of white matter integrity and quantitative evaluations of its damage have become possible using the DTI technique. The use of this technique is supported by several previous studies that have evaluated various neurological diseases [11–16].

We found that all the values of the mean FA for the selected association fibers in FTD patients were significantly decreased. Because these fibers connect the temporal lobe with other cortices, they are believed to play an important role in verbal, cognitive and emotional functions. Thus, damage to these vital tracts may result in aphasia, memory disturbance or personality disorders, which are symptoms frequently observed in FTD. The decrease in FA in the left UF was significantly correlated with CDR and MMSE score, possibly indicating that the FA value for this particular tract may reflect the patient's clinical stage. A previous experimental study has shown that disruption of the UF results in severe memory impairment [28]. The cortices of these areas are those that are mainly affected and damaged in FTD. Thus, the FA value in this area may be the only one that enables monitoring of the severity of FTD.

In contrast to the UF, the degree of the decrease in FA in the AF and ILF appeared not to be significantly correlated with the clinical stage of FTD, although the FA value in the left ILF showed a decrease in most FTD patients with aphasia. It has recently been hypothesized that the temporal pole and anterior fusiform gyrus could be a part of a semantic network that might be underlain by the ILF [29]. Using the method of DTI, allowing in vivo dissection of white matter fibers [30], recent studies have confirmed the classical anatomical description (direct pathway) and also defined U-shaped fibers of the occipitotemporal projection system (indirect pathway) [22]. Mandonnet et al. recently reported that semantic paraphasia could be induced by the direct electrical stimulation on the ILF in patients with glioma [31]. Our results indicate that the FA values in the ILF and AF may be decreased in FTD from an early stage. In the study by Borroni et al. patients with tvFTD showed white matter reductions in the ILF [2]. This result is in accordance with ours. Thus the decreased anisotropy of the ILF and UF may reflect one of the pathophysiological features of FTD.

Atrophy of the CC has been also discussed in relation to cognitive impairment [32], and a conventional MR study has shown that predominant atrophy of the genu is a

characteristic of patients with FTD [33]. In our study, the decrease in the FA value in the genu of the CC was greater than in the splenium, supporting the previously reported data. On the other hand, FA values in the pyramidal tracts of FTD patients were relatively high. This indicates that projection fibers are preserved in FTD even in the advanced stage. These findings suggest that the distribution of CWM damage in FTD is not uniform, and thus association fibers that are related to the frontotemporal as well as temporooccipital lobes, and anterior commissural fibers, are more selectively damaged in FTD than projection fibers.

If the characteristic features of FTD can be elucidated by DTI, this method may become helpful for the differential diagnosis of other neurodegenerative diseases characterized by dementia, especially AD. Although the difference between AD and FTD has already been discussed from the viewpoints of clinical symptoms and conventional radiological findings [34, 35], FA measurement by DTI may provides a new approach for understanding both diseases. Taoka et al. evaluated the "tract of interest" by diffusion tensor tractography and TSM in patients with AD and found that the FA values in the bilateral UF and left inferior occipitofrontal fasciculus were decreased [36]. In our study, the mean FA values in the bilateral UF of FTD patients was also significantly lower than in the controls. In addition, we detected a decrease in the mean FA values in the AF and ILF in FTD patients. These fasciculi have never been assessed in any study of AD. If more striking differences in CWM changes between FTD and AD can be demonstrated by DTI at an early clinical stage, DTI may be helpful in differential diagnosis.

However, there were some limitations to this study. Since we investigated a limited number of patients, a definite conclusion about the clinical applicability of DTI cannot be reached at present. In order to establish the connection between DTI findings and clinical disease, it will be necessary to demonstrate a clinicoradiological correlation in a larger number of patients. Secondly, neuropathological comparison of CWM damage was not possible because we were unable to obtain any autopsy cases. Larsson et al. were able to perform an autopsy on a patient with FTD and found moderate frontal white matter gliosis with demyelination, suggesting a correlation between the DTI data for the formalin-fixed brain and the histopathology [37]. It will be necessary to verify this point in a larger number of patients with FTD in order to support the utility of DTI.

In conclusion, by tractography-based analysis, we were able to demonstrate quantitatively the features of FTD that affected association fibers and anterior fibers of CC in the CWM of FTD patients, which showed a decrease in FA in comparison with the control group. These findings suggest that FTD is associated with pathological changes not only in the cerebral cortex but also in the CWM. Therefore, DTI may be a useful tool for detecting this aspect of FTD, and may provide important clues for elucidating the underlying pathogenesis of the disease.

Conflict of interest statement We declare that we have no conflict of interest.

References

1. The Lund and Manchester Groups (1994) Clinical and neuropathological criteria for frontotemporal dementia. J Neurol Neurosurg Psychiatry 57:416–418
2. Borroni B, Brambati SM, Agosti C, Gipponi S, Bellelli G, Gasparotti R et al (2007) Evidence of white matter changes on diffusion tensor imaging in frontotemporal dementia. Arch Neurol 64:246–251
3. Cooper PN, Siddons CA, Mann DM (1996) Patterns of glial cell activity in fronto-temporal dementia (lobar atrophy). Neuropathol Appl Neurobiol 22:17–22
4. Nichol KE, Kim R, Cotman CW (2001) Bcl-2 family protein behavior in frontotemporal dementia implies vascular involvement. Neurology 56 [Suppl 4]:S35–S40
5. Schofield E, Kersaitis C, Shepherd CE, Kril JJ, Halliday GM (2003) Severity of gliosis in Pick's disease and frontotemporal lobar degeneration: tau-positive glia differentiate these disorders. Brain 126:827–840
6. Martin JA, Craft DK, Su JH, Kim RC, Cotman CW (2001) Astrocytes degenerate in frontotemporal dementia: possible relation to hypoperfusion. Neurobiol Aging 22:195–207
7. Kitagaki H, Mori E, Hirono N, Ikejiri Y, Ishii K, Imamura T et al (1997) Alteration of white matter MR signal intensity in frontotemporal dementia. AJNR Am J Neuroradiol 18:367–378
8. Catani M, Piccirilli M, Cherubini A, Tarducci R, Sciarma T, Gobbi G et al (2003) Axonal injury within language network in primary progressive aphasia. Ann Neurol 53:242–247
9. Basser PJ, Mattiello J, LeBihan D (1994) Estimation of the effective self-diffusion tensor from the NMR spin echo. J Magn Reson (B) 103:247–254
10. Pierpaoli C, Basser PJ (1996) Toward a quantitative assessment of diffusion anisotropy. Magn Reson Med 36:893–906
11. Ellis CM, Simmons A, Jones DK, Bland J, Dawson JM, Horsfield MA et al (1999) Diffusion tensor MRI assesses corticospinal tract damage in ALS. Neurology 53:1051–1058
12. Aoki S, Iwata NK, Masutani Y, Yoshida M, Abe O, Ugawa Y et al (2005) Quantitative evaluation of the pyramidal tract segmented by diffusion tensor tractography: feasibility study to patients with amyotrophic lateral sclerosis. Radiat Med 23:195–199
13. Yoshikawa K, Nakata Y, Yamada K, Nakagawa M (2004) Early pathological changes in the parkinsonian brain demonstrated by diffusion tensor MRI. J Neurol Neurosurg Psychiatry 75:481–484
14. Takahashi S, Yonezawa H, Takahashi J, Kudo M, Inoue T, Tohgi H (2002) Selective reduction of diffusion anisotropy in white matter of Alzheimer disease brains measured by 3.0 Tesla magnetic resonance imaging. Neurosci Lett 332:45–48
15. Rose SE, Chen F, Chark JB, Zelaya FO, Strugnell WE, Benson M (2000) Loss of connectivity in Alzheimer's disease: an evaluation of white matter tract integrity with colour coded MR diffusion tensor imaging. J Neurol Neurosurg Psychiatry 69:528–530
16. Shiga K, Yamada K, Yoshikawa K, Mizuno T, Nishimura T, Nakagawa M (2005) Local tissue anisotropy decreases in

cerebellopetal fibers and pyramidal tract in multiple system atrophy. J Neurol 252:589–596
17. Yoshiura T, Mihara F, Koga H, Noguchi T, Togao O, Ohyagi Y et al (2006) Cerebral white matter degeneration in frontotemporal dementia detected by diffusion-weighted magnetic resonance imaging. Acad Radiol 13:1373–1378
18. Catani M (2006) Diffusion tensor magnetic resonance imaging tractography in cognitive disorders. Curr Opin Neurol 19:599–606
19. Conturo TE, Lori NF, Cull TS, Akbudak E, Snyder AZ, Shimony JS et al (1999) Tracking neuronal fiber pathways in the living human brain. Proc Natl Acad Sci U S A 96:10422–10427
20. Catani M, Jones DK, Ffytche DH (2005) Perisylvian language networks of the human brain. Ann Neurol 57:8–16
21. Kiel EL, Staib LH, Davis LM, Bronen RA (2004) MR imaging of the temporal stem: anatomic dissection tractography of the uncinate fasciculus, inferior occipitofrontal fasciculus, and Meyer's loop of the optic radiation. AJNR Am J Neuroradiol 25:677–691
22. Catani M, Jones DK, Donnato R, Ffytche DH (2003) Occipito-temporal connections in the human brain. Brain 126:2093–2107
23. McKhann GM, Albert MS, Grossman M, Miller B, Dickson D, Trojanowski JQ (2001) Clinical and pathological diagnosis of frontotemporal dementia: report of the Work Group on Frontotemporal Dementia and Pick's Disease. Arch Neurol 58:1803–1809
24. Morris J (1993) The Clinical Dementia Rating (CDR): current version and scoring rules. Neurology 43:2412–2414
25. Wakana S, Jiang H, Nagae-Poetscher LM, van Zijl PC, Mori S (2004) Fiber tract-based atlas of human white matter anatomy. Radiology 230:77–87
26. Basser PJ, Pierpaoli C (1996) Microstructural and physiological features of tissues elucidated by quantitative-diffusion-tensor MRI. J Magn Reson B 111:209–219
27. Le Bihan D, Turner R, Douek P, Patronas N (1992) Diffusion MR imaging: clinical applications. AJR Am J Roentgenol 59:591–599
28. Gaffan D, Easton A, Parker A (2002) Interaction of inferior temporal cortex with frontal cortex and basal forebrain: double dissociation in strategy implementation and associative learning. J Neurosci 22:7288–7296
29. Vigneau M, Beaucousin V, Hervé PY, Duffau H, Crivello F, Houdé O et al (2006) Meta-analyzing left hemisphere language areas: phonology, semantics, and sentence processing. Neuroimage 30:1414–1432
30. Catani M, Howard RJ, Pajevic S, Jones DK (2002) Virtual in vivo interactive dissection of white matter fasciculi in the human brain. Neuroimage 17:77–94
31. Mandonnet E, Nouet A, Gatignol P, Capelle L, Duffau H (2007) Does the left inferior longitudinal fasciculus play a role in language? A brain stimulation study. Brain 130:623–629
32. Yamauchi H, Fukuyama H, Ogawa M, Ouchi Y, Kimura J (1994) Callosal atrophy in patients with lacunar infarction and extensive leukoaraiosis: an indicator of cognitive impairment. Stroke 25:1788–1793
33. Yamauchi H, Fukuyama H, Nagahama Y, Katsumi Y, Hayashi T, Oyanagi C et al (2000) Comparison of the pattern of atrophy of the corpus callosum in frontotemporal dementia, progressive supranuclear palsy, and Alzheimer's disease. J Neurol Neurosurg Psychiatry 69:623–629
34. Sinagawa S, Ikeda M, Fukuhara R, Tanabe H (2006) Initial symptoms in frontotemporal dementia and semantic dementia compared with Alzheimer's disease. Dement Geriatr Cogn Disord 21:74–80
35. Miller BL, Gearhart R (1999) Neuroimaging in the diagnosis of fronto-temporal dementia. Dement Geriatr Cogn Disord 10 [Suppl 1]:71–74
36. Taoka T, Iwasaki S, Sakamoto M, Nakagawa H, Fukusumi A, Myochin K et al (2006) Diffusion anisotropy and diffusivity of white matter tracts within the temporal stem in Alzheimer disease: evaluation of the "Tract of Interest" by diffusion tensor tractography. AJNR Am J Neuroradiol 27:1040–1045
37. Larsson EM, Englund E, Sjöbeck M, Latt J, Brockstedt S (2004) MRI with diffusion tensor imaging post-mortem at 3.0 T in a patient with frontotemporal dementia. Dement Geriatr Cogn Disord 17:316–319

Neuropathology 2008 doi:10.1111/j.1440-1789.2008.00996.x

Original Article

In vivo expression of proinflammatory cytokines in HIV encephalitis: an analysis of 11 autopsy cases

Hui Qin Xing,[1] Hitoshi Hayakawa,[1,2] Kimiko Izumo,[1] Ryuji kubota,[1] Ellen Gelpi,[2] Herbert Budka[2] and Shuji Izumo[1]

[1]Division of Molecular Pathology, Center for Chronic Viral Diseases, Graduate School of Medical and Dental Sciences, Kagoshima University, Sakuragaoka, Kagoshima, Japan, and [2]Neurological Institute, Medical University Vienna, Vienna, Austria

As the pathogenesis of AIDS dementia complex (ADC), cytokines such as TNF-α and IL-1β have been thought to have toxic effects on CNS cells and induce neuronal cell death. However, many of the discussions have been based on the studies done by in vitro experiments. There are only a few reports which demonstrate proinflammatory cytokines directly in vivo in HIV encephalitis (HIVE) brains, and roles of these cytokines with relation to HIV-1 infection are not yet clarified. In the present study, we examined 11 autopsy cases of HIVE using immunohistochemistry, and explored which cell types expressed these cytokines and whether expression of cytokines was related to viral infection. IL-1β was detected in the frontal white matter of all 11 cases where microglial nodules were observed to varying degrees, whereas TNF-α was detected in seven cases. IL-1β– or TNF-α-positive cells were almost restricted to CD68-positive macrophages/microglia and mild expression of these cytokines by astrocytes was observed in two cases with severe HIVE. IL-1β was detected in some HIVp24-positive multinucleated giant cells. However, we could not detect TNF-α expression in the HIVp24-positive cells, which indicates that IL-1β is induced by HIV-1 infection. In conclusion, a macrophage/microglia lineage is the main cell type to release cytokines in HIVE, and IL-1β expression by HIV-1-infected cells may be one of the important factors for induction of HIVE. In addition, many non-infected macrophages/microglia as well as some astrocytes express IL-1β and TNF-α, which might contribute to pathogenesis of ADC.

Key words: HIV encephalitis, HIVp24, IL-1β, multinucleated giant cells, TNF-α.

INTRODUCTION

AIDS dementia complex (ADC)[1,2] is a clinical triad of progressive cognitive decline, motor dysfunction, and behavioral abnormalities induced by human immunodeficiency virus 1 (HIV-1), and occurs in approximately 20% of AIDS cases during the late stages of the HIV-1 infection.[3] One of the histopathologic correlates of ADC is diffuse and nodular microgliosis with formation of multinucleated giant cells (MNGCs) in the white mater of the brain and is termed HIV encephalitis (HIVE),[4–6] Myelin pallor[4] and axonal damage[7–9] with abundant HIV-infected macrophages and microglial cells have been demonstrated in the white mater.[4,10] However, poor correlations between these findings and the clinical manifestations of ADC have been repeatedly reported.[11,12] On the other hand, diffuse poliodystrophy (DPD) has been reported as another histopathologic evidence for ADC,[4,5] and a variety of neuronal damages such as neuronal loss, apoptosis of neurons, and synaptic and dendritic simplification have been demonstrated in the cerebral cortex.[4,5,13–19]

Our previous study using a Simian immunodeficiency virus (SIV)-infected macaque model demonstrated that two types of pathologic changes, an inflammatory process with virus-infected multinucleated giant cells in the white matter and degenerative changes of the cerebral cortex along with development of immunodeficiency, could occur

Correspondence: Hui Qin Xing, MD, PhD, Division of Molecular Pathology, Center for Chronic Viral Diseases, Graduate School of Medical and Dental Sciences, Kagoshima University, 8-35-1 Sakuragaoka, Kagoshima 890-8544, Japan. Email: xhqw63@hotmail.com

Received 8 September 2008; revised 27 October 2008 and accepted 6 November 2008.